Dinoflagellate cyst paleoecology during the Pliocene–Pleistocene climatic transition in the North Atlantic

Jan A. I. Hennissen[a,b,*], Martin J. Head[a,c], Stijn De Schepper[d], Jeroen Groeneveld[e]

[a]*Department of Earth Sciences, University of Toronto, 22 Russell Street, Toronto, Ontario M5S 3B1, Canada*

[b]*British Geological Survey, Nicker Hill, Keyworth, Nottingham, NG12 5GG, United Kingdom*

[c]*Department of Earth Sciences, Brock University, 1812 Sir Isaac Brock Way, St. Catharines, Ontario L2S 3A1, Canada*

[d]*Uni Research Climate, Bjerknes Centre for Climate Research, Nygårdsgaten 112–114, N-5008 Bergen, Norway*

[e]*MARUM – Center for Marine Environmental Sciences, University of Bremen, Klagenfurter Strasse, D-28359 Bremen, Germany*

[*]Corresponding author. Tel: +44(0) 115 936 3532.

E-mail address: janh@bgs.ac.uk (J. Hennissen).

Abstract

Dinoflagellate cysts (dinocysts) are widely used as tracers of sea surface conditions in late Quaternary marine records. However, paleoenvironmental reconstructions across the Pliocene–Pleistocene climatic transition and beyond are limited because the hydrologic conditions influencing assemblage compositions may not have a modern analogue, and the ecological optima of extinct dinocyst species are not well known. From a study of two cored sites in the central and eastern North Atlantic, we bypass these issues by statistically analyzing the variations in dinocyst assemblage composition and comparing the results directly to paleoecological parameters ($\delta^{18}O_{bulloides}$, $\delta^{18}O_{salinity}$, and geochemical proxies for sea surface temperature [SST]) derived from the planktonic foraminifer *Globigerina bulloides* recovered from the same samples as the dinocysts. Through canonical correspondence analysis we demonstrate the co-variation of seasonality and dinocyst paleoproductivity. We show that *Pyxidinopsis braboi* is a cold tolerant species with an optimum SST between 12 and 14 °C. We extend the use of *Nematosphaeropsis labyrinthus* as an indicator of transitional climatic conditions to the Pliocene, we offer evidence for the correlation of *Bitectatodinium tepikiense* and *Filisphaera microornata* to high seasonality, and we reiterate an apparent link between *Spiniferites mirabilis* and eastern North Atlantic water masses. Finally, we confirm that *Habibacysta tectata* is cold-tolerant rather than a strictly cold-water indicator, that *Operculodinium*? *eirikianum* is a cold-intolerant species favoring outer neritic environments, and that *Ataxiodinium confusum* and *Invertocysta lacrymosa* are both warm-water species.

1 Introduction

Recent decades have seen an emphasis on Neogene and Quaternary paleoceanographic reconstructions based on dinoflagellate cyst (dinocyst) research. This follows groundbreaking work on the ecological calibration of extant dinocysts by Wall et al. (1977). With the distribution patterns of species in modern surface sediments clearly linked to variations in environmental parameters (e.g. Harland, 1983), data from such distributions were projected onto fossil assemblages in an effort to document paleoclimatic changes in a (semi)quantitative way (e.g. Edwards et al., 1991; Mudie, 1992). Since then, extensive databases of modern dinocyst distributions have been compiled (e.g. Rochon et al., 1999; de Vernal et al., 2001; Radi and de Vernal, 2008) and have led to a substantially increased understanding of the dinocyst assemblage–environment relationship. These databases have been used to develop dinocyst-based transfer functions utilizing the best modern analogue technique (e.g. de Vernal et al., 1997; de Vernal et al., 1992). The methodology, despite its caveats (Telford, 2006; Telford and Birks, 2009, 2011), produces generally plausible and detailed reconstructions of late Quaternary deposits (de Vernal et al., 2005; de Vernal et al., 2001; Radi and de Vernal, 2008) but has important limitations when applied to older Quaternary and Neogene dinocyst records. On geological time scales, evolution becomes potentially a significant factor, and it can be questioned whether the ecological parameters controlling modern species distributions are comparable to those for fossil species distributions, a basic assumption in quantitative paleoclimatology (Birks, 1995, 2003; Imbrie and Kipp, 1971). It is also true that the full range of environmental factors controlling modern distributions is probably incompletely known, and it would be unreasonable to presume that recent environments provide analogues for all past paleoenvironments (Dale, 1996). Moreover, for assemblages of Early Pleistocene age and older, the presence of extinct species may prevent a modern analogue from being identified. Finally, it must be accepted that from the surface waters in which they were formed to their final incorporation into the sedimentary record, the cysts must have undergone some lateral transport both within the water column and during any subsequent remobilization by bottom-water currents.

To mitigate some of these caveats, we use a same-sample technique, developed by De Schepper et al. (2009), that combines foraminiferal geochemistry (Mg/Ca, $\delta^{18}O$) with marine palynology. This methodology allows the direct correlation of sea-surface parameters (sea surface temperature (SST) and

sea surface salinity (SSS)) with major changes in the dinocyst assemblages. Furthermore, data acquired in this way offer invaluable information on SST constraints for extinct species (e.g. De Schepper et al., 2011). To assess the ecological conditions influencing the dinocyst assemblages and their constituent species across the Pliocene–Pleistocene boundary, we utilized the data sets of Hennissen et al. (2014, 2015) for two sites in the eastern North Atlantic: Deep Sea Drilling Project (DSDP) Site 610 in the path of the North Atlantic Current (NAC), and Integrated Ocean Drilling Program (IODP) Site U1313 at the northern margin of the North Atlantic Subtropical Gyre (Figure 1). In the current study, we present a statistical analysis, based on the ecological model of Dale and Dale (2002), to analyze down-core palynological records using independently acquired paleoenvironmental information to:

- Elucidate the ecological constraints of extinct dinocyst species, including *Ataxiodinium confusum, Filisphaera microornata*, *Habibacysta tectata*, *Invertocysta lacrymosa*, *Operculodinium*? *eirikianum* and *Pyxidinopsis braboi.*
- Constrain the Pliocene ecological parameters of extant dinocyst species, including *Bitectatodinium tepikiense, Impagidinium pallidum, I. aculeatum, Nematosphaeropsis labyrinthus* and *Spiniferites mirabilis*.

2 Material and Methods

2.1 Samples

Samples (15 cc) were collected from DSDP Hole 610A and IODP Hole U1313C (Figure 1). Hole 610A is located on the Feni Drift (53°13'N; 18°53'W; water depth 2417 m), a 600 km long and 500 m thick sediment drift containing deposits dating back to the Early Miocene (Dowling and McCave, 1993; Stoker et al., 2005). IODP Hole U1313C (41°00'N; 32°57'W), drilled at a water depth of 3426 m (Expedition 306 Scientists, 2006), is a reoccupation of DSDP Site 607. In Hole 610A, the studied interval from 2782 to 2565 ka is constrained by the age model of Hennissen et al. (2014). For Hole U1313C, the age model of Bolton et al. (2010) is used to constrain the sampled interval from 2784 ka to 2524 ka.

Standard palynological maceration techniques detailed in Hennissen et al. (2014) were used to isolate the organic matter in the recovered samples. Residues were sieved at 10 μm and mounted on microscope slides using glycerine jelly. One *Lycopodium clavatum* tablet (batch no. 177745) was added to each sample as a spike to determine dinocyst concentrations (Stockmarr, 1971) and the dinocyst burial flux (DBF)

(Hennissen et al., 2014; Versteegh et al., 1996). The counts for Holes 610A and U1313C are summarized in supplementary Tables ts01 and ts02 respectively, published here for the first time. Resulting abundances for the most frequently encountered species are given in Figures 2 and 3.

2.2 Data handling

Before conducting the statistical analysis, we excluded unidentified dinocysts (dinocyst spp.) from the counts because of the lack of a diagnostic taxonomic basis other than the presence of an archeopyle or other traces of tabulation. The distribution pattern of this group is not driven by a taxon-specific affinity for certain ecological parameters and thus carries no relevant paleoecological information.

Sample 15-2a in Hole 610A is the only sample with a significant relative abundance of *Operculodinium centrocarpum* sensu Wall and Dale 1966–short processes (5%; Table ts01). This taxon forms a morphological series with *O. centrocarpum* sensu Wall and Dale (1966) (Harland, 1973) and even though salinity plays a role in process length, as shown by the global dataset of Mertens et al. (2009) and in modern waters of the Baltic Sea (Jansson et al., 2014; Sildever et al., 2015), an obvious relationship has not been demonstrated in the Plio-Pleistocene sediments from the North Atlantic. We therefore grouped both morphotypes together following Rochon et al. (1999).

Bitectatodinium tepikiense and *Filisphaera microornata* share morphological similarities and they are believed to have similar ecological niches in the Pliocene North Atlantic (Head et al., 1993; Head et al., 1989a). However, the genus *Filisphaera* became extinct in the Middle Pleistocene (Head et al., 1993) whereas *B. tepikiense* is an extant species (Zonneveld et al., 2013), implying that *Filisphaera* and *Bitectatodinium* have slightly different ecological requirements. In the current study we distinguished two morphotypes of *Bitectatodinium tepikiense*: *B. tepikiense* (columellate) and *B. tepikiense* (vermiculate) (Head et al., 2004). Because we observed that *B. tepikiense* (vermiculate) and *F. microornata* form a morphological series, they were grouped together. *Bitectatodinium tepikiense* (columellate) was kept apart for CCA and SST vs. abundance analyses in Hole 610A. Because of the low abundances and subtlety of diagnostic criteria, the morphotypes of *B. tepikiense* were not separated in Hole U1313C and for this hole we combined *B. tepikiense* with *F. microornata* for subsequent statistical analyses.

Spiniferites mirabilis and *S. hyperacanthus* were grouped together as the *Spiniferites mirabilis* group because of their comparable morphology (de Vernal et al., 1992) and the difficulty in distinguishing one from the other when unfavourably oriented (Rochon et al., 1999). The resulting tables that were then used for the ensuing statistical analysis are Tables ts03 and ts04. All taxa, with their abbreviations, used in the current manuscript are listed in Table 1.

2.3 Statistical analysis of the dinoflagellate cyst assemblages

Two main ordination methods exist to relate species abundance data to environmental factors. The linear ordination method assumes a linear response of species abundance to the availability of a limiting environmental variable. In contrast, a unimodal species response assumes a Gaussian distribution around a maximum abundance, which reflects the optimum value of a limiting factor for a given species (Hutchinson, 1957; ter Braak, 1985; ter Braak and Prentice, 1988; Whittaker, 1967). To establish the appropriate ordination method for our data, we used detrended correspondence analysis (DCA). In this technique, developed by Hill and Gauch (1980), the lengths of the gradients of variation in abundance are taken as the range of the sample scores. The length is expressed in standard deviation units (SD) and it is assumed that each taxon's abundance rises to its maximum, falls and returns to zero within 4 SD (Hill and Gauch, 1980). If the longest gradient length is shorter than 3 SD, the taxon's response is considered to change linearly with the environmental gradient and a linear ordination model is employed (Birks, 1995). If the gradient length is longer than 3 SD, a unimodal species response is assumed and a unimodal ordination is generally considered a better choice to minimize the arching effect in modeling the abundance data (Leps and Smilauer, 2003).

The variation shown by the axes (gradients of variation) in DCA is caused by one or a combination of environmental factors, which explains the position of samples and species in the resulting diagram. For the samples in this study, a large amount of environmental information is already available which may facilitate DCA interpretation. Additionally, with this information we can place environmental constraints on the acquired species' distribution by forcing the ordination axes to be linear combinations of these known environmental variables, a technique called detrended canonical correspondence analysis (DCCA) when used for unimodal ordination models and canonical correspondence analysis (CCA) for linear ordination models (ter Braak, 1986). In (D)CCA we utilized information on eight variables listed below.

Based on the mixed-layer dwelling planktonic foraminifer *Globigerina bulloides*, recovered from the same samples as the dinocysts, the following environmental variables for Holes 610A and U1313 were measured by Hennissen et al. (2014):

1. **Sea surface temperature (SST)** derived from the Mg/Ca composition of the planktonic foraminifer *G. bulloides*.
2. The **$\delta^{18}O_{bulloides}$ (= $\delta^{18}O_{bul}$) values** measured on the tests of *G. bulloides*.
3. **Sea surface salinity** estimates $\delta^{18}O_{salinity}$ (= $\delta^{18}O_{sal}$) based on the $\delta^{18}O_{bul}$ record corrected for SST and global ice volume, using Lisiecki and Raymo (2005).
4. For Hole U1313C only, Hennissen et al. (2015) derived a **seasonality index** based on the SST difference between estimates from *G. bulloides* specimens (Hennissen et al., 2014) and *Globigerinoides ruber* (white) *sensu stricto* from the record published by Friedrich et al. (2013).

From the dinocyst abundances in Holes 610A and U1313 (Hennissen et al., 2014), we calculated ecological ratios following Versteegh (1994) and Versteegh and Zonneveld (1994):

5. The ratio between **inner neritic and oceanic species (IN/O).** The species used to calculate this ratio are listed in Table 2.
6. The ratio between **outer neritic and oceanic species (ON/O).** The species used to calculate this ratio are listed in Table 2.

As an approximation of dinocyst paleoproductivity, we took:

7. The **Dinocyst Burial Flux** from Hennissen et al. (2014).

Following Versteegh and Zonneveld (1994), we utilized:

8. **Age** as a measure for the environmental and biological evolution during the studied time slab.

Counts were conducted until at least 300 dinocyst specimens were identified, or in the case of 21 very low concentration samples in Hole U1313C (Table ts02), until two complete microscope slides had been counted. The raw counts were converted to relative abundances for subsequent statistical analyses, executed in R version 3.0.2 (R Core Team, 2013). The *decorana* routine of the *vegan* package for

community ecology (Oksanen et al., 2013) performs DCA in R whereas the *cca* routine from the same package with values for the eight ecological parameters (Tables ts03 and ts04) was used for (D)CCA.

3 Results

3.1 (Detrended) Correspondence Analysis

The primary gradients of DCA in Hole 610A for the samples (3.00 SD) and species (4.49 SD) are larger than or equal to 3 standard deviations suggesting a unimodal ordination to be appropriate to model species response. For Hole U1313C, the primary DCA gradients of samples (2.29 SD) and species (3.83 SD) suggest that a linear ordination is more appropriate following the recommendations of Birks (1995) and Leps and Smilauer (2003).

3.1.1 DCA in Hole 610A

The eigenvalues for the first four axes of DCA and the species scores for these axes are summarized in Table 3. The first two DCA axes have eigenvalues of 0.499 and 0.340 (Figure 4). The most influential species in the studied interval is *Operculodinium centrocarpum* sensu Wall and Dale (1966) (*O. centrocarpum* from hereon, but in fact the cyst of *Protoceratium reticulatum* according to Paez-Reyes and Head, 2013), reflected by the statistical weight (30.961), nearly six times higher than the weight of the second most influential taxon, *Spiniferites* spp. indet. *Operculodinium centrocarpum* plots at the negative end of the first axis while *Pyxidinopsis braboi* plots at the positive end (Figure 4). Species that plot on the positive end of DCA 1 tend to be separated more effectively by DCA 2 than species on the negative end of DCA 1, which all plot in the -1–1 interval for DCA 2. Samples derived from the interval prior to Marine Isotope Stage (MIS) G1 generally plot on the negative end of DCA 1 while samples from MIS 104–102 plot on the positive end (Figure 5). At the positive end of DCA 1, samples are well separated by DCA 2, while at the negative end, samples cluster together and have low DCA 2 scores. The second DCA axis effectively separates samples belonging to the older MIS G1–MIS 104 interval from samples belonging to the younger MIS 103–102. This distribution shows the strong influence of the most abundant species in the assemblages, *O. centrocarpum*: samples rich in *O. centrocarpum* plot on the left of Figure 5, while samples (almost) devoid of *O. centrocarpum* plot on the right.

3.1.2 CA in Hole U1313C

Table 4 shows the eigenvalues for the first four CA axes and the corresponding CA species scores. The first CA axis separates *Invertocysta lacrymosa* at one end of the spectrum from the *S. mirabilis* group at the other end (Figure 6). The second CA axis separates *I. lacrymosa* and the *S. mirabilis* group from the rest of the assemblages, while the spread of all other abundant species in Hole U1313C is contained within a narrow band of -1–1. The oldest samples from the studied interval (MIS G9–G7) all plot on the negative end of CA1 and the positive end of CA2, showing the influence of *I. lacrymosa* (Figure 7). Samples from the MIS G2–104 interval plot on the positive end of CA1 and CA2 reflecting the higher abundance of the *S. mirabilis* group. During MIS 104, *O. centrocarpum* is more abundant in the assemblages and this is shown in the negative CA1 scores. From MIS 103 to MIS 100, samples score low on CA1 and are generally negative on CA2.

3.2 Canonical Correspondence Analysis

In CCA, the axes are forced to be linear combinations of measured variables, each of which is depicted in the figures as an arrow with its length expressing the explanatory power for its individual variable. The angle between the species or sample and the arrow representing the environmental variable expresses the degree of correlation between the species/sample and the variable. For CCA, we focus on the species that are most abundant in each of the two holes, these having the highest statistical weight after the DCA/CA (species in bold in Tables 3 and 4). The CCA in Hole 610 A and U1313C are summarized in Figures 8–11.

3.2.1 CCA in Hole 610A

The eigenvalues of the first two CCA axes are 70% and 49% respectively of the eigenvalues of the first two DCA axes (Table 5) testifying that the measured environmental parameters have an important influence on species and sample distributions. Age has the greatest relative length and smallest angle with respect to the CCA1 axis (Figures 8–9). Other parameters positively correlated to CCA1 are ON/O and DBF. Sea surface temperature, IN/O and $\delta^{18}O_{sal}$ are closely correlated, all negatively to both axes. The $\delta^{18}O_{bul}$ arrow has a narrow angle with the positive side of the second axis.

3.2.2 CCA in Hole U1313C

Eigenvalues for the first two CCA axes are 83% and 67% of the first two CA axes respectively, showing that the measured environmental variables influence the distribution of species and samples (Figures 10–11). The environmental parameters plot in three separate clusters. The DBF, $\delta^{18}O_{bul}$ and IN/O correlate

negatively with CCA1 and positively with CCA2 while seasonality correlates positively with both axes. Sea surface temperature, $\delta^{18}O_{sal}$ and age all correlate negatively with CCA2, with SST correlating with the positive domain of CCA1. The ON/O index correlates closely with CCA1 and plots negatively compared to CCA2.

4 Discussion

4.1 Lateral transport

Ecological concepts for dinoflagellate cysts in paleopalynology assume that the recovered sediments contain cyst assemblages which reflect the dinoflagellate assemblage in the water column above. This assumption in practice must allow for no more than limited lateral transport influencing the in-situ assemblage. The present record contains four lines of evidence that point to our assemblages broadly reflecting the prevailing surface water conditions (see also Hennissen et al., 2014).

(1) Neither a dominance nor an increase of inner neritic or estuarine species was recorded during peak glacial conditions, even though lowered sea levels would be expected to have introduced assorted cysts deposited on surrounding shelves during earlier glacial and interglacial intervals. In particular, *Lingulodinium machaerophorum* and *Spiniferites bentorii*, which are common coastal species of the temperate area (Wall et al., 1977; Dale et al., 2002; Zonneveld et al. 2013), were not found to increase during peak glacial intervals. *Operculodinium centrocarpum* is a cosmopolitan but somewhat more offshore species with higher abundances at the convergence of oceanic and neritic water masses (Dale and Dale, 2002), but it is also very common throughout the range of water depths in the North Atlantic (e.g. Wall et al., 1977; Harland, 1984) and it is unlikely that its elevated abundance results solely from displacement. Moreover, an abundance increase of *O. centrocarpum* from near the coast to outer shelf has been observed in waters off the western coast of South Africa by Davey and Rogers (1975), whereas Zonneveld et al. (2013) observed high abundances in both coastal and deep-sea samples.

(2) There is a distinct rarity of protoperidiniacean cysts in the assemblages. These cysts are abundant in coastal temperate regions (Wall et al., 1977) and would be present in higher abundances if displacement of near-shore material had occurred. Of all dinoflagellate cysts, protoperidiniaceans are the most sensitive to oxidation, but the removal of protoperidiniaceans by oxidation is unlikely judging from

the excellent preservation of the rare specimens present and of other dinoflagellate cysts, and the relatively high abundances of amorphous organic matter throughout both holes.

(3) The samples contain very few pollen or spores. The D-P index (Versteegh 1994; Versteegh and Zonneveld 1994; De Schepper et al., 2009) for Hole 610A averages 0.97 with a minimum of 0.90 and a maximum of 1.00 (Table ts01). For Hole U1313C these scores were the same: 0.90 (0.97) 1.00 (Table ts02). These very high values indicate a limited influence of coastal sediments.

(4) Reworked marine palynomorphs were recorded in very low abundances: in Hole 610A the highest reworking rate (3%) occurred at 2675 ka with 12 reworked specimens for 376 in-situ cysts (Table ts01), whereas in Hole U1313C a maximum reworking rate of 2% was recorded at 2530 ka (Table ts02) with five identifiably reworked specimens for 309 recorded in-situ cysts. The overall scarcity of reworked palynomorphs indicates insignificant input from either shelf or distant oceanic areas. The somewhat higher amounts of reworked palynomorphs in Hole 610A during MIS G8, G6 and the MIS G4–G3 boundary are concurrent with peaks of IRD (Kleiven et al., 2002) and could be related to the melting of icebergs (Figure 12).

In addition, we are ecologically calibrating the cysts not with the characteristics of surface waters but with foraminifers that may have shared somewhat similar transport pathways. Foraminifera are larger than dinoflagellate cysts, but settling rates may not have been very different given that cysts are thought to fall rapidly to the sea floor through flocculation and agglomeration (Mudie, 1996).

4.2 Dinocyst Paleoproductivity

For the North Atlantic basin, several databases have been developed to quantify productivity from dinocyst concentrations in modern surface sediments (Devillers and de Vernal, 2000; Radi and de Vernal, 2008). In the fossil record, dinocyst burial flux (DBF) can be used as an indicator of paleoproductivity (Versteegh et al., 1996), and it is at least theoretically a better indicator than dinocyst concentration because it adjusts for governing sedimentation rates (Hennissen et al., 2014). At Site 607/U1313, dinocyst concentrations (Hennissen et al., 2014; Versteegh et al., 1996) and the flux of alkenones (Naafs et al., 2010) are in-phase with each other, but show higher values during glacials, when reduced productivity might be expected. Versteegh et al. (1996) proposed that these peaks in dinocyst concentration are a consequence of an

introduction of nutrient-rich waters following changes in atmospheric circulation during glacial intervals. When dinocyst concentration is compared to the DBF for Hole 610A (Figure 12b), which is excellently located to track the NAC, a discrepancy between the two can be seen during MIS 104. Dinocyst concentrations peak but the DBF fails to reach levels recorded during the preceding glacials of the sampled interval. Hence, paleoproductivity as indicated by the DBF is much lower than suggested by dinocyst concentration during MIS 104 when seasonality, as indicated at Site U1313, is at a maximum (Figure 12b). Concurrently, *Pyxidinopsis braboi* reached its acme in Hole 610A and replaced the previously abundant NAC indicator *O. centrocarpum* (Figure 2h, l). Because the extant Gulf Stream–NAC system is known to convey elevated levels of nutrients to the northern North Atlantic (Pelegrí et al., 1996; Rintoul and Wunsch, 1991), the high DBF and high relative abundance of *O. centrocarpum* at Site 610A during the glacials preceding MIS 104 reflect an active NAC at these times. During MIS 104, the DBF discrepancy and the disappearance of *O. centrocarpum* together show an interrupted NAC and associated decline in nutrient flux. In contrast, the increased DBF and dinocyst concentration at Site U1313 during MIS 104 show a persistent NAC over the mid-latitudes of the North Atlantic (Figure 12d). Because the inferred southward shift of the NAC and decline in paleoproductivity at Site 610 all occur during MIS 104, and do so at a time of apparently increased seasonality (Hennissen et al., 2015), they could have a common cause.

4.3 The position of the Arctic Front in the study area during the iNHG

The Arctic Front (AF) separates the warm saline waters of the NAC and the Irminger Current from the cold Arctic waters, and is considered to mark the maximum extent of the winter sea-ice in the modern Nordic Seas (Swift and Aagaard, 1981). For the present study area, Hennissen et al. (2014) hypothesized a position of the AF close to Hole 610A during MIS 104 based on the replacement of *O. centrocarpum* by the cold tolerant species *P. braboi*, possibly driven by an elevated atmospheric pressure over the expanding circum-Atlantic ice sheets. Other evidence of the closeness of the AF to Site 610 comes from $\delta^{13}C_{bul}$ which reflects more local changes in the composition of the mixed layer of the water column and is mainly driven by the amount of nutrients (Broecker and Peng, 1988) and photosynthetic activity which can be linked to paleoproductivity: photosynthetic organisms preferentially take up ^{12}C, leaving the reservoir enriched in ^{13}C (Sarnthein et al., 1988; Zahn et al., 1986). Hence, an increase in paleoproductivity is reflected by a rise in $\delta^{13}C_{bul}$. In Hole 610A, peaks of DBF indeed correspond to peaks in $\delta^{13}C_{bul}$ and IRD (Kleiven et al.,

2002) for the interval MIS G9–G1 (Figure 12a, b), but not for MIS 104 (Section 4.2). In Hole U1313C, a remarkable correspondence between DBF, seasonality and $\delta^{13}C_{bul}$ is observed for the interval MIS G9–G1 (Figure 12c, d): increases in paleoproductivity, indicated by DBF, correspond to peaks in seasonality and $\delta^{13}C_{bul}$. At the end of MIS 104, a sudden drop in $\delta^{13}C_{bul}$ co-occurs with a peak rather than a drop in paleoproductivity. This most likely corresponds with the introduction of a different water mass linked to a southward shift of the NAC and AF, evidenced by the replacement of *O centrocarpum* by *P. braboi* in Hole 610A (Figure 2) and the first sustained glacial peak of IRD-sourced material at Site U1313 (Figure 12c) (Naafs et al., 2013). Because paleoproductivity and seasonality remain in phase in Hole U1313C (Figure 12, d), it seems that the seasonal contrast in SST is the main driver of paleoproductivity in the study area.

4.4 Detrended correspondence analysis in Hole 610A

The first axis in the DCA of Hole 610A (Figure 4) separates samples with high abundances of *O. centrocarpum* from samples rich in *P. braboi* that plot at the other end of the spectrum and are almost entirely contained within MIS 104 (Figures 2h, l). This could be interpreted as a reflection of the influence of the NAC (Section 4.2). Around interglacial G7, *O. centrocarpum* declines in abundance and is replaced by the warm-tolerant (Head, 1996; Head et al., 1989a) *O.*? *eirikianum* (Figure 2k, l), possibly in response to the slightly higher SST (Figure 13a).

The DCA2 axis, although important in explaining variability in the dinoflagellate cyst assemblages as indicated by the high eigenvalue (Table 3), is difficult to interpret. Samples belonging to MIS G1 and MIS 103–102 are separated effectively, while the older samples from the section (MIS G8–G6) cluster closer together at the negative end of DCA 1. This is reflected in the changes of DCA 2 values through the sampled section (Figure 13d): DCA 1 remains low to slightly positive in the interval that is dominated by *O. centrocarpum*, whereas it drops to negative values at the MIS G2–G1 boundary simultaneously with a rise in relative abundance of *B. tepikiense* (vermiculate)+ *F. microornata* (Figure 2a), and reaches a minimum during MIS 104 concurrent with the acme of *P. braboi*. Therefore, DCA 2 most likely reflects an interplay of oceanic/oligotrophic (*I. aculeatum*) and cold/nutrient-elevated (*P. braboi*) influences.

4.5 Correspondence analysis in Hole U1313C

The CA1 axis in Hole U1313C (Figure 6) separates the *Spiniferites mirabilis* group and *Invertocysta lacrymosa* from all other recorded species. The CA1 axis is negative (Figure 13e) in the interval with high abundances of *I. lacrymosa* and exhibits positive excursions when the *S. mirabilis* group and *O. centrocarpum* (MIS 104) reach high abundances (MIS G2 and 104; Figure 3h, j). The *S. mirabilis* group plots in relative isolation, with none of the species with high statistical weights plotting close to its position. This could point towards a source for *S. mirabilis* that is different from the main association and corroborates the findings of Versteegh (1997) that these high abundances represent incursions of different water masses.

At the other end of the CA1 axis, *Invertocysta lacrymosa* again plots in isolation, with none of the species having high statistical weights plotting close to its position. *Invertocysta lacrymosa* is a warm water species typical of open oceanic conditions (De Schepper et al., 2011; Versteegh and Zonneveld, 1994). Its extinction is recorded in the studied interval (Section 4.7.1.2), which explains its isolation in the multivariate analysis. The first CA axis reflects the separation of the two end members from all other species that plot close to each other: the *S. mirabilis* group, because of the suggested incursion of different water masses, and *I. lacrymosa* because of its limited range in the sampled interval.

The CA2 axis in Hole U1313C again separates *I. lacrymosa* and the *S. mirabilis* group, at the positive end of the axis, from all the other species (Figures 6 and 13e). Both taxa are also positively correlated to SST with all occurrences of *I. lacrymosa* in a range of 18.8–22.7°C and the highest relative abundances of the *S. mirabilis* group occurring between 21 and 22°C (Figure 16). The only other species to plot positively compared to DCA2 is *O. centrocarpum*. It has high abundances during MIS 104 when a southward move of NAC is hypothesized to a position close to Site U1313 (Section 4.3). *Nematosphaeropsis labyrinthus* plots close to *O. centrocarpum* and becomes important in the succession from MIS G2 onwards with peaks near the MIS 104–103, MIS 102–101 and MIS 101–100 boundaries (Section 4.6.1.4). This suggests a negative correlation with SST and it is reflected in the most negative CA2 values for the most common species in U1313C. Therefore, we interpret the CA2 axis as a SST-dependent axis.

4.6 Canonical correspondence analysis and the paleoecology of Pliocene dinocyst assemblages

To unravel the major influences responsible for the dinocyst abundance signatures, we performed a canonical correspondence analysis integrating the independently derived paleoceanographic parameters SST(Mg/Ca), $\delta^{18}O_{sal}$, $\delta^{18}O_{bul}$, and the non-hydrographic parameter DBF based on the *Lycopodium* spike method corrected for sedimentation rate. For the data from Hole U1313C (Figures 10–11), we included seasonality as determined by Hennissen et al. (2015). We will discuss the paleoecological behavior of the species that have statistical weights in the upper quartile as indicated in Table 3 (Hole 610A) and Table 4 (Hole U1313C). We do not consider taxa in open nomenclature (*Spiniferites* spp. indet., *Filisphaera/Pyxidinopsis* spp. indet., *Spiniferites ramosus/delicatus*?, *Invertocysta* sp. 1 and *Impagidinium* spp. indet.) because their uncertain taxonomic affinity could compromise the paleoecological interpretation.

4.6.1 Variance and co-variance of the ecological parameters

In both holes, high values of $\delta^{18}O_{sal}$ are associated with low SST (Figures 14–16). This reflects the major influence of the ice volume effect on the isotopic composition of the foraminifera in the North Atlantic. The non-hydrographic parameter DBF is closely related to high $\delta^{18}O$ values in the planktonic foraminifer tests confirming the increased paleoproductivity during glacial intervals as observed by Versteegh et al. (1996) and Hennissen et al. (2014). Additionally, the independently derived seasonality co-varies strongly with DBF (Figure 12). This result suggests that a rise in seasonality can be correlated with a peak in the paleoproductivity of cyst-forming dinoflagellates (Section 4.2).

4.7 The Paleoecology of selected Pliocene and Pleistocene dinocysts

In the discussion below we separate the autecology of species based on their influence on the statistical analysis into those species with statistical weighs in the upper quartile in both holes, and then those in the upper quartile only in 610A or U1313C. Lastly, we discuss selected taxa registered only in low numbers. An overview of the paleoceanographic significance of the recorded taxa is provided in Table 6.

4.7.1 Species with statistical weights in the upper quartile in both holes

4.7.1.1 Operculodinium centrocarpum sensu Wall and Dale (1966) (Plate 1, Figures 1–2)

Operculodinium centrocarpum occurs in high abundances in Hole 610A (>60%) throughout the entire observed SST (8–16°C) and $\delta^{18}O_{sal}$ (-0.03–2.51 ‰) ranges (Figure 14). In the CCA from Hole 610A, a strong correlation with age and DBF becomes apparent. *Operculodinium centrocarpum* is the dominant

species from MIS G9 to MIS 104, thereafter disappearing from the record until MIS 102 when it reappears in relatively low abundances (Figure 2l). Studies of modern North Atlantic dinoflagellate cyst distributions (e.g. Dodge and Harland, 1991; Harland, 1983; Rochon et al., 1999; Wall et al., 1977; Williams, 1971) show *O. centrocarpum* as the dominant cyst species along a broad path closely reflecting the position of the North Atlantic Current (NAC), and the distribution of its motile stage shows a similar pattern (Matthiessen et al., 2005). The modern North Atlantic and indeed global distributions of *O. centrocarpum* reveal it to be a cosmopolitan species living within a wide variety of temperatures and salinities (de Vernal et al., 2001; Zonneveld et al. 2013), absent only from areas of permanent ice cover (Mudie, 1992). *Operculodinium centrocarpum* tolerates unstable conditions caused by the mixing of neritic and oceanic waters along continental margins (Dale, 1996), and indeed Dale and Dale (2002) related high abundances of *O. centrocarpum* to the neritic–open ocean convergence zone in the southern part of the Atlantic Ocean. This species has been used as a proxy for NAC influence in down-core studies of the Pliocene and Pleistocene in the eastern North Atlantic (De Schepper et al., 2009; De Schepper et al., 2013; Hennissen et al., 2014). In the present study, we interpret high abundances of *O. centrocarpum* as reflecting the influence of the NAC. In Hole U1313C, *O. centrocarpum* occurs over the entire range of SSTs (Figure 16), with the highest abundance (29%) occurring during MIS 104 consistent with the southward shift of the NAC, close to Site U1313. In the CCA of U1313C, *O. centrocarpum* plots near the centre, confirming that it is not influenced by one environmental parameter in particular, which is the behavior expected from a cosmopolitan, opportunistic species.

4.7.1.2 Invertocysta lacrymosa (Plate 1, Figures 3–4)

The extinction of *Impagidinium lacrymosa* is one of the main biostratigraphic markers in the planktonic realm during the intensification of Northern Hemisphere Glaciation (iNHG) (De Schepper et al., 2009; de Vernal and Mudie, 1989; Harland, 1979; Versteegh, 1997) and is most likely related to the first phase of cooling during the iNHG. The highest occurrence of this species in Holes 610A (2728 ka) and U1313C (2752 ka) causes a strong correlation with age in the CCA from both holes (Figures 8 and 10). Analyses of the optimal SST ranges for *I. lacrymosa* in both holes show a clear positive relationship with SST (Figures 14 and 16). *Invertocysta lacrymosa* is interpreted as a warm water species typical of open oceanic

conditions (see also De Schepper et al., 2011; Versteegh and Zonneveld, 1994) with its highest occurrence datum within the studied interval of both holes.

4.7.1.3 Impagidinium aculeatum (Plate 1, Figures 5–7)

Impagidinium aculeatum correlates positively with SST in the CCA of both holes (Figures 8, 10, 15, 16). The SST range analysis shows increased abundance with increasing SST (Figures 15, 16). Abundances are lower in Hole 610A (maximum 25% when SST is 15.4 °C) than in U1313C (>80% in the 20–22 °C interval), emphasizing the overall higher SSTs in the latter and presumably also more oligotrophic conditions. Indeed, in Hole U1313C, *I. aculeatum* is negatively correlated with ON/O, IN/O and DBF, supporting its affinity for oligotrophic waters (see also Devillers and de Vernal, 2000; Wall et al., 1977). This relationship is less clear in Hole 610A where *I. aculeatum* seems to be positively correlated to IN/O (Figures 8 and 10), although it is negatively correlated to ON/O and DBF. This can be explained by the positive correlation between the inner neritic (Versteegh and Zonneveld, 1994) species *Tectatodinium pellitum* and SST. Because *I. aculeatum* also correlates to the positive end of SST, and IN/O in Hole 610A (Table 2) is mainly influenced by the thermophilic *T. pellitum* (Harland, 1983; Head, 1994), an artificially strong relationship appears between *I. aculeatum* and IN/O. Therefore, we interpret *I. aculeatum* as a warm oligotrophic species near the Plio-Pleistocene boundary. In modern waters, *Impagidinium aculeatum* is common in the North Atlantic waters where winter and summer SSTs are >12°C and >18°C respectively and surface salinity exceeds 35 (Rochon et al., 1999).

4.7.1.4 Nematosphaeropsis labyrinthus (Plate 1, Figures 9–11)

For the North Atlantic realm during the Pleistocene, this species has been shown to represent transitional climatic conditions during times when profound changes in water mass composition occurred (Baumann and Matthiessen, 1992; Eynaud et al., 2004; Eynaud et al., 2000; Penaud et al., 2008). In the present study, we extend this observation into deeper time with a peak abundance in Hole 610A (48% at 2587 ka) occurring during a major dinoflagellate cyst turnover in response to a fundamental change in water masses as indicated by the increase in $\delta^{18}O_{bul}$, a drop in SST, and an increase in seasonality (Figure 12b, c). In Hole 610A, two abundance peaks of *N. labyrinthus* near the MIS G1–104 and MIS 104–103 transitions envelop the acme of *P. braboi* (Figure 2 h, i). The negative correlation of *N. labyrinthus* with DBF and ON/O suggests tolerance of oligotrophic waters as reported also by Devillers and de Vernal (2000) and

Turon and Londeix (1988) (Figures 8, 10). In their overview of 371 sites across the North Atlantic, Devillers and de Vernal (2000) associated peaks of *N. labyrinthus* with low SST. However, the SST analysis of *N. labyrinthus* in Hole 610A of the current study (Figure 14) suggests a positive relationship with SST because abundance increases as SST rises (positive correlation in CCA, Figures 8, 10). In Hole U1313C, *N. labyrinthus* becomes progressively more important throughout the studied interval (Figure 3k) with a maximum abundance of 47% at 16.2°C, which results in a CCA-scoring that reflects an affinity for cold SSTs and more nutrient enriched waters (Figure 10). Upon combining the information from both holes, it is clear that in Hole 610A only the lower half of the SST spectrum of *N. labyrinthus* is represented whereas the broader SST range recorded in U1313C reveals the unimodal distribution of abundance versus SST (Figure 16) with an optimal SST around 16 °C. This corresponds well with the abundances described in other Pliocene studies where maximum abundances (>60%) are registered around 15 °C (De Schepper et al., 2011).

4.7.1.5 The *Spiniferites mirabilis* group (Plate 1, Figures 12–13)

In Hole 610A, the abundance of this taxon never exceeds 3% suggesting that climatic conditions were at the fringes of its environmental range. In the more southerly located Hole U1313C, abundances are much higher and a positive relationship with SST is seen, with the highest abundances (>50%) occurring between 21 and 22°C (Figure 16) which reflect the affinity of this group for warmer waters as described in earlier studies (e.g. Harland, 1983; Rochon et al., 1999). The CA1 axis in Hole U1313C (Figure 6) separates the *Spiniferites mirabilis* group (and *Invertocysta lacrymosa*) from all other recorded species within the upper quartile. In the extant oceans, *Spiniferites mirabilis* and *S. hyperacanthus* are recorded in high abundances in the eastern North Atlantic (Harland, 1983; Rochon et al., 1999; Zonneveld et al., 2013). The isolation of the *S. mirabilis* group in the statistical analyses of the abundances of Hole U1313C indeed points to a source for this taxon that differs from other taxa, and supports the hypothesis of Versteegh (1997) that these high abundances represent incursions of a different water mass, either from the Bay of Biscay or the Mediterranean Sea where *S. mirabilis* also occurs in higher abundances (Eynaud et al., 2004).

In the modern oceans, the *Spiniferites mirabilis* group is reported in most samples from the eastern North Atlantic and off the eastern margins of the United States (Harland, 1983). Rochon et al. (1999) considered

this a warm, oceanic group tolerant of winter SSTs exceeding 13°C and salinities exceeding 34.5. Zonneveld et al. (2013) described *S. mirabilis* as having a temperate to equatorial distribution, occurring in both coastal and oceanic environments. It has been reported from permanently or seasonally reduced-salinity environments (Zonneveld et al., 2013).

4.7.1.6 Bitectatodinium tepikiense and *Filisphaera microornata* (Plate 1, Figures 14–20; Plate 2, Figures 1–4)

In Hole 610A, the DCA of the *B. tepikiense* (vermiculate) +*F. microornata* group and *B. tepikiense* (columellate) plot similarly along the DCA1 axis, but they are separated along the CA2 axis (Figure 4). Notably, both *B. tepikiense* (vermiculate) +*F. microornata* group and *B. tepikiense* (columellate) have their highest abundances between 12 and 14 °C, are correlated negatively with age (Figure 8), and show a drop in abundance at around 14 °C after which higher abundances are again recorded up to 16 °C after which *B. tepikiense* (columellate and vermiculate) and *F. microornata* all but disappear from the assemblages (Figure 14). In Hole U1313C, *B. tepikiense* is closely correlated to seasonality and negatively to SST (Figure 10). The SST vs. abundance analysis in Hole U1313C (Figure 16) confirms that *F. microornata* and *B. tepikiense* are associated with low temperatures and reduced salinity conditions reflecting this groups' tolerance of cool conditions as noted by Head et al. (1989a) and Head et al. (1993). Upon combining the information of both holes we see that the highest abundances of *B. tepikiense* (vermiculate and columellate) and *F. microornata* occur when the NAC and Arctic Front moved southward during MIS 104 (Hennissen et al., 2014). Higher abundances of *B. tepikiense* have already been associated with increased water stratification (Mudie, 1992) and seasonality (de Vernal et al., 2005) and possibly the proximity of the Polar Front (Bakken and Dale, 1986; Dale, 1985). Separating *B. tepikiense* (vermiculate) from *B. tepikiense* (columellate) for statistical analyses in Hole 610A has not revealed major differences in ecological requirements for the two morphotypes. Some separation occurs along the DCA2 axis (Figure 4) which is difficult to interpret but most likely reflects an interplay of oceanic/oligotrophic (*I. aculeatum*) and cold/nutrient-elevated (*P. braboi*) influences. In this light, *B. tepikiense* (columellate) plots closer to oceanic/oligotrophic species (*Impagidinium* spp. indet., cysts of *P. dalei*, and *I. paradoxum*) than *B. tepikiense* (vermiculate) + *F. microornata*. It should be borne in mind that whereas *B. tepikiense* is an extant species, *F. microornata* is extinct and must have had different ecological requirements, these presumably including a lower tolerance of cold waters.

In modern waters, *Bitectatodinium tepikiense* has maximum occurrences in temperate to sub-Arctic conditions of the North Atlantic region: e.g. the bays of Nova Scotia (Mudie, 1992) and Maine (Wall et al., 1977). Because of its maximum occurrence at the mouth of the St. Lawrence drainage system, Rochon et al. (1999) regarded *B. tepikiense* as having an affinity for stratified surface waters characterized by large seasonal SST amplitudes (up to 18 °C) combined with relatively low salinities (30–32). Zonneveld et al. (2013) suggested that *B. tepikiense* is restricted to sub-polar and temperate areas. It is reported in seasonally ice-covered areas (less than 4 months/year; de Vernal et al., 1997) and Bakken and Dale (1986) hypothesized high abundances related to the proximity of the Polar Front.

4.7.1.7 Impagidinium paradoxum (Plate 2, Figures 5–9)

Impagidinium paradoxum plots near *I. aculeatum* in the CCA plots of Hole 610A reflecting its affinity for warmer, oligotrophic waters (Figure 8). However, the optimum SST for maximum *I. paradoxum* abundances is lower than for *I. aculeatum* (Figure 15). The broader SST spectrum recorded in Hole U1313C shows that the highest abundance (53%) of *I. paradoxum* occurs when the SST is 13.2°C, and relative abundances abruptly decline (<15%) when SST exceeds 21°C (Figure 16). The different SST intervals in both holes explain the positive correlation between SST and *I. paradoxum* in Hole 610A yet negative correlation in U1313C (Figures 8, 10): the total unimodal distribution of *I. paradoxum* is truncated in the SST spectrum of 610A whereas the SST spectrum of U1313C completely covers its rise, optimum and decline. In modern sediments, *Impagidinium paradoxum* has been observed with abundances exceeding 10% in North Atlantic sediments south of 50°N (Harland, 1983) and exceeding 20% when the SST is higher than 12°C (Radi and de Vernal, 2008). Here we consider it an oligotrophic species characteristic of higher SSTs, but with a SST optimum lower than that of *I. aculeatum*.

4.7.2 Species with statistical weights from the upper quartile in Hole 610A

4.7.2.1 Pyxidinopsis braboi (Plate 2, Figures 10–15)

The first axis in the DCA of Hole 610A (Figure 4) separates samples with high abundances of *O. centrocarpum* from samples rich in *P. braboi*, which plot at the other end of the spectrum. *Pyxidinopsis braboi* reaches abundances in excess of 40 % in a fairly narrow SST range (~12–14 °C). It is mostly associated with relatively cold conditions; although it occurs in low numbers within the cool to warm-temperate neritic assemblages from the Pliocene of Belgium (De Schepper and Louwye 2004; De

529 Schepper et al., 2009, and as *Pyxidinopsis* sp. 1 in Louwye et al., 2004), possibly temperate neritic
530 assemblages from the lowermost Pleistocene (Ludhamian = lower Gelasian) of eastern England
531 (questionably as *Filisphaera* sp. cf. *F. filifera* in Head, 1996), and in Hole U1313C in the current study. It
532 is one of the earliest species to appear in sediments from the Miocene of Antarctica after an extended
533 barren interval representing a period of continuous ice cover (Warny et al., 2009). Hennissen et al. (2014)
534 hypothesized its association with the Arctic Front in the North Atlantic. We consider *Pyxidinopsis braboi* a
535 cold tolerant species with high abundances in MIS 104 perhaps reflecting elevated nutrient levels
536 associated with the Arctic Front.

537 *4.7.2.2 Operculodinium? eirikianum* (Plate 2, Figures 16–20)
538 *Operculodinium? eirikianum* is positively correlated with age, DBF and ON/O (Figure 8). Its abundance
539 signature is similar to that of *O. centrocarpum* (Figure 2k, l) except in MIS G7 when it reaches its highest
540 abundances (up to 16%) during the decline of *O. centrocarpum*. It disappears from the record in MIS 104
541 during the iNHG, as also noted by De Schepper and Head (2008). The CCA plot reveals no particular
542 negative or positive relationship with SST, as reflected also in the scattered SST range plot (Figure 14).
543 *Operculodinium? eirikianum* has been described as a cold-intolerant species with an affinity for outer
544 neritic to oceanic environments (Head, 1996; Head et al., 1989b). Because of the low abundances (<5%) in
545 the coldest part of the section (<10 °C), its highest occurrence during iNHG, and the positive correlation
546 with ON/O, our results are consistent with the cold intolerant, outer neritic character of this species.

547 *4.7.2.3 Habibacysta tectata* (Plate 3, Figures 1–2)
548 In CCA, *Habibacysta tectata* correlates positively with SST, IN/O and $\delta^{18}O_{sal}$. It has high abundances in
549 the 12.5–15.7 °C SST range, with highest abundances primarily occurring under low $\delta^{18}O_{sal}$ conditions
550 (Figure 15). The highest abundances (around 50%) occur during MIS 103 when *O. centrocarpum*
551 disappeared from the assemblages and *N. labyrinthus* rose significantly in abundance. *H. tectata* has been
552 described as a cool-tolerant (Head, 1994; Head et al., 1989c) or cold water (De Schepper et al., 2011;
553 Versteegh, 1994; Versteegh, 1997) species, and De Schepper et al. (2011) demonstrated its cool-water
554 affinities. The reason for its positive correlation with SST in the CCA of the current study is the narrow
555 total SST range (8–16 °C) of the studied interval in Hole 610A. The lower part of this range lies below the
556 optimum SST of *H. tectata*, with no occurrences, while the upper part coincides with the optimum SST of

this species. The apparent positive correlation between SST and *H. tectata* abundance (Figure 15) is therefore a result of the limited record which does not incorporate the full SST range for this species. In fact, the optimum SST range of *H. tectata* in the current study corresponds well with the observations of De Schepper et al. (2011) who noted that abundances in excess of 30% are usually recorded in intervals with a SST between 10 and 15 °C. Given this optimal SST range, its distribution in the late Cenozoic of the Gulf of Mexico, and the fact that it probably did not survive beyond the Early Pleistocene (Head et al., 2004), we confirm that *H. tectata* is not strictly a cold water indicator but more precisely a cool-tolerant species with an affinity for cool waters (De Schepper et al., 2011; Head, 1994b; Head et al., 1989c). It is likely that SST is not the only ecological factor influencing the distribution of *H. tectata*. The CCA analysis shows a strong positive correlation between *H. tectata* and $\delta^{18}O_{sal}$ (Figure 8) which means that in Hole 610A more saline waters are associated with higher abundances of this species.

4.7.2.4 Impagidinium pallidum (Plate 3, Figures 3–6)

Despite being in the upper quartile of the DCA, *Impagidinium pallidum* does not occur frequently in Hole 610A (maximum abundance of 7%). It plots close to the centre in the CCA (Figure 8), and correlates slightly positively with $\delta^{18}O_{sal}$, SST and IN/O. The SST/abundance analysis (Figure 15) suggests increasing abundances with increasing SST, with maximum abundance occurring at 15.2 and 15.8 °C during MIS 102 and MIS G8. These results are in accord with the Pliocene–Lower Pleistocene temperature distribution of this species (De Schepper et al., 2011) which points to a tolerance of warmer waters than its present distribution (de Vernal et al., 1994; Matthiessen and Knies, 2001) would suggest. The results of CCA show that the distribution of this species near the Pliocene–Pleistocene boundary is not necessarily driven by a single factor, though it has its highest abundances in a narrow interval around 16 °C.

In the modern oceans, *Impagidinium pallidum* is observed in (sub-)arctic environments with an active oceanic gyre, with maximum abundances reported from the central Greenland Sea (Matthiessen, 1995). *Impagidinium pallidum* has been reported also from the Gulf of Alaska (de Vernal and Pedersen, 1997), the southern Indian Ocean (Marret and de Vernal, 1997) and the Beaufort Sea (Mudie, 1992). Rochon et al. (1999) associated *I. pallidum* with cold winter conditions and summer temperatures ranging from 0–8°C with salinities between 30 and 34. These authors concluded that *I. pallidum* may be a good indicator of cold sea-surface conditions at open oceanic sites. Zonneveld et al. (2013) regarded *I. pallidum* as a polar

585 species occurring with high relative abundances in sites that are seasonally covered by sea ice and which
586 experience seasonally reduced salinities.

587 *4.7.2.4* Cysts of *Pentapharsodinium dalei* (Plate 3, Figure 7)
588 Cysts of *Pentapharsodinium dalei* exhibit an abundance signature (Figure 2c) and SST range analysis plot
589 (Figure 14) similar to those of *I. pallidum*, with maximum abundances of 7% occurring at SSTs around
590 15.5 °C during MIS 102. Consequently, its position in the CCA plot (Figure 8) is close to that of *I.*
591 *pallidum* but slightly more towards $\delta^{18}O_{bul}$. Because of its affinity for higher $\delta^{18}O_{bul}$ and abundances that
592 exceed 5% in waters with a SST ranging from 10.8 to 15.7 °C we view *P. dalei* as a cold tolerant species in
593 Hole 610A.

594 This extant species dominates modern assemblages in Norwegian fjords (as ?*Scrippsiella* in Dale, 1976; as
595 *Peridinium faeroense* in Dale, 1977), where it is considered an indicator of sheltered coastal waters
596 (Bakken and Dale, 1986). It is a spring-blooming species, and is considered to be approaching the upper
597 limit of its temperature tolerance in the Oslofjord of southern Norway (Dale, 2001). It has been interpreted
598 as a cold water species because it has been found in waters that were covered by ice for up to twelve
599 months per year (de Vernal et al., 1997; Harland and Pudsey, 1999). Rochon et al. (1999) showed from its
600 North Atlantic distribution that this species occurs when summer SST exceeds 4°C and becomes important
601 under large seasonal SST gradients. Zonneveld et al. (2013) regarded this taxon as a polar to equatorial,
602 euryhaline, cosmopolitan species with high abundances in all environments with the exception of arctic
603 regions.

604 4.7.3 Species with statistical weights from the upper quartile in Hole U1313C
605 *4.7.3.1 Pyxidinopsis tuberculata* (Plate 3, Figures 8–9)
606 *Pyxidinopsis tuberculata* occurs in low abundances (maximum of 8%) throughout the sampled interval
607 (Figure 3g) in Hole U1313C. In the CCA, *P. tuberculata* plots close to the center with a slight positive
608 correlation with higher SST and $\delta^{18}O_{sal}$. The SST/abundance analysis reveals that *P. tuberculata* has
609 highest abundances (6–8 %) within a range of 16–22 °C (Figure 15). This is higher than the range of 9.0–
610 16.5 °C given by De Schepper et al. (2011). In that study, however, the maximum recorded abundance of
611 *P. tuberculata* is only 3%. Similar abundances have been observed in the current study for SSTs lower
612 than 16 °C (Figure 16). The CCA of Hole U1313C (Figure 10) shows a negative correlation to both IN/O

and ON/O which means it occurs in higher abundances in more oceanic and oligotrophic conditions. We view *P. tuberculata* as having a slight preference for more saline, higher temperature and open oceanic waters.

4.7.3.2 Impagidinium patulum (Plate 3, Figures 10–12)

Impagidinium patulum is present in fairly low abundances throughout the sampled interval in Hole U1313C, occurring in most samples. Its highest abundance of 7% is recorded during MIS 102 when the SST was around 18 °C (Figures 3f, 16). In the CCA, this species plots close to the center (Figure 10) but distinctly opposite ON/O. The SST analysis reveals the occurrence of *I. patulum* over the entire range of SSTs and $\delta^{18}O_{bul}$. Harland (1983) showed *I. patulum* occurring in abundances below 10% across the North Atlantic and the Mediterranean, whereas Zonneveld et al. (2013) showed high abundances only when SST is above 20°C in winter and exceeds 25°C in summer. In our study of the Pliocene North Atlantic, abundances may reach 5% when SST reaches 15°C. Following CCA and SST range analysis, we view *I. patulum* as an open-ocean species tolerating a wide range of hydrographic conditions but does not exceed 7% where SSTs are below 22°C.

4.7.4 Rare species with paleoenvironmental implications

Aside from the most abundant species, discussed above, we present the autecology of three additional species because they have proven to be good paleoenvironmental indicators despite occurring in very low abundances. These species are *Ataxiodinium confusum*, *Corrudinium*? *labradori* and *Tectatodinium pellitum*.

4.7.4.1 Ataxiodinium confusum (Plate 3, Figures 13–15)

Ataxiodinium confusum occurs in Hole 610A in low abundances (less than 2 %) and it is broadly positively correlated to SST (Figure 15). The CCA of Hole 610A shows a strong correlation with age, which could mean its highest occurrence is recorded in the current study which is in line with De Schepper and Head (2010) and with findings in western North Atlantic Hole 603C (Head, pers. obs.). The SST spectrum of *A. confusum* in Hole U1313C reveals abundances over 2% in the 18–22 °C interval. The CCA of U1313C shows a strong correlation with SST and age (Figure 10). Here, the correlation with age is a result of the co-occurrence of *A. confusum* with the highly age dependent warm-water species *I. lacrymosa*. Hence, we

640 view *A. confusum* as a warm water indicator as has been proposed also by Udeze and Oboh-Ikuenobe
641 (2005) and De Schepper et al. (2011).

642 *4.7.4.2 Corrudinium? labradori*
643 *Corrudinium*? *labradori* was recovered only from Hole U1313C. Its maximum abundance of 2.6% is
644 reached at a SST of 20°C, and the SST spectrum in Hole U1313C (Figure 16) shows a broadly positive
645 correlation with SST that is confirmed by CCA (Figure 10). It had been suggested that SST was not the
646 main control for its distribution (De Schepper et al., 2011), but that data from colder regions was lacking.
647 In the current study, *C.*? *labradori* does not occur in the cooler Hole 610A, which could indicate a
648 temperature control. However, *C.*? *labradori* has been recovered from intervals within the SST spectrum
649 of Hole 610A, even at SST below 10°C (De Schepper et al., 2011). Because it correlates negatively with
650 both IN/O and ON/O in the CCA of U1313C (Figure 10), this could indicate that *C.*? *labradori* is an
651 oligotrophic, open oceanic species and its absence in Hole 610A could then be a result of the presence of
652 the nutrient-rich NAC for a large part of the interval. More data from intervals rich in *C.*? *labradori* are
653 required to confirm this hypothesis.

654 *4.7.4.3 Tectatodinium pellitum* (Plate 3, Figures 16–17)
655 In Hole 610A, *T. pellitum* surpasses 1.5% only when SST exceeds 12°C, and in the CCA this known
656 thermophile (Head, 1994) is indeed correlated positively with SST. These abundances are not reached in
657 Hole U1313C where it only occurs (<1%) in a narrow SST range of 18–19°C. These low abundances in
658 the oceanic Hole U1313C may be explained by long-distance transport given the mainly inner neritic
659 distribution of this species (Versteegh and Zonneveld, 1994 and Table 2). We regard *T. pellitum* as an
660 inner neritic species with a positive correlation to SST.

661 In the modern oceans *Tectatodinium pellitum* is regarded as a coastal subtropical to equatorial species with
662 highest relative abundances in meso- to eutrophic waters (Zonneveld et al., 2013).

663 # 5. Future work
664 The current study shows the value of conducting extensive palynological counts on samples that are also
665 used for geochemical (Mg/Ca and $\delta^{18}O$) analysis on foraminiferal tests, under the assumption that the
666 dinoflagellates and foraminifers share the same habitat (De Schepper et al., 2011) and that lateral transport
667 is of limited influence (Section 4.1). The fluctuations in relative abundances of dinoflagellate cysts reveal

at a glance the important changes taking place during MIS 104, but it is only after conducting DCA, CCA and SST versus abundance analysis that the ecological optima of the various dinocyst taxa can be objectively established. The combination of proxies clearly highlights the proximity of NAC and the Arctic Front (*O. centrocarpum* and *P. braboi*; Figure 4), biostratigraphical constraints (*I. lacrymosa*, *A. confusum*; Figure 6) and the incursions of water masses with different ecological conditions (*S. mirabilis* group; Figure 6).

The same sample approach combined with the applied statistical modeling also emphasizes the importance of the DBF to assess paleoproductivity. Because DBF incorporates sedimentation rate, it is a much better indicator of productivity than cyst concentration, as we have shown for MIS 104 of DSDP 610A (Section 4.1). The total values of DBF also aid interpretation of basinal setting: DBF is much lower for the open oceanic Hole U1313C than it is for the more proximal Hole 610A. However, the influence of transported cysts on paleoproductivity assessments, especially in areas of low productivity, needs to be tracked carefully (Dale and Fjellså, 1994) using the paleoecological knowledge of the cysts within the studied record. The statistical approaches on down core data, as presented in the current study, will improve constraints on the paleoecological optima of extant and extinct dinocyst species. This in turn will lead to a better understanding of dinocyst paleoproductivity and its links to increased seasonality in the Early Pleistocene.

To test the above hypotheses and the paleoecological constraints imposed on Pliocene–Pleistocene dinoflagellate cysts in the current study, it is necessary that a similar same-sampling technique combined with comparable statistical analyses is conducted on other holes in the North Atlantic domain. Figure 1 gives an overview of all the nearby holes that have cored the same interval as the one discussed in the current study. This could serve as a starting point for further refinement in understanding the paleoecology of dinoflagellate cysts in the Pliocene and Pleistocene.

6 Conclusions

We analyzed palynological and hydrological data acquired from the same samples from an interval across the Pliocene–Pleistocene (Neogene–Quaternary) boundary in two North Atlantic boreholes: DSDP Hole 610A (2782–2565 ka) and IODP Hole U1313C (2784–2524 ka). These holes have independent SST and

other environmental variables based on foraminiferal geochemistry obtained from the same sample set as that used for dinocyst analysis. We utilized (detrended) correspondence analysis and canonical correspondence analysis to identify the main ecological parameters responsible for the observed species distributions. In the ecological dataset we included SST, $\delta^{18}O_{bul}$, $\delta^{18}O_{sal}$, ratios of inner and outer neritic to oceanic species (IN/O and ON/O) and dinocyst burial flux (DBF). For Hole U1313C, we included seasonality (using data from Hennissen et al., 2015) as an additional ecological parameter.

We have shown that the application of ecological concepts on paleontological data, as presented by Dale and Dale (2002), can provide constraints in understanding the ecological responses of both extant and extinct species during the Pliocene and Pleistocene. In particular, we have found that:

- A strong link exists between the DBF as a proxy for paleoproductivity and the peak of seasonality during MIS 104, indicating a possible common cause.
- Peaks in abundance of *Bitectatodinium tepikiense* + *Filisphaera microornata* can be correlated to increases in seasonality in Hole U1313C. No significant difference in SST requirements between the morphotypes *B. tepikiense* (columellate) and *B. tepikiense* (vermiculate) are seen. However, the columellate morphotype may be related to more oceanic/oligotrophic conditions than the vermiculate morphotype.
- *Pyxidinopsis braboi* is confirmed as a cold tolerant species with a SST optimum in the 11.7–13.8 °C range. It is strongly linked to the southward movement of the Arctic Front during MIS 104, perhaps in response to elevated nutrient levels.
- *Habibacysta tectata* has a positive correlation with SST in Hole 610A that confirms this species as cold-tolerant rather than a strictly cold water indicator, in keeping with other geological evidence for this extinct species.
- The affinity of *Nematosphaeropsis labyrinthus* for rapidly changing water masses, proven for Pleistocene intervals, extends into the Pliocene. The optimum SST during iNHG is recorded around 16 °C.

- *O. centrocarpum* sensu Wall and Dale (1966) while showing a response consistent with its association with the NAC, is influenced by multiple ecological parameters as expected of a cosmopolitan, opportunistic species.
- *Invertocysta lacrymosa* is interpreted as a warm water species typical of open ocean conditions.
- The *Spiniferites mirabilis* group when abundant appears to represent incursions of discrete water masses presumably sourced from the eastern North Atlantic.
- *Impagidinium paradoxum* is an oligotrophic species characteristic of elevated SSTs but with an optimum lower than that of *I. aculeatum*.
- The distribution of *Operculodinium*? *eirikianum* in our material is consistent with the cold-intolerant, outer neritic character of this species as determined from other studies.
- *Ataxiodinium confusum* although occurring in low abundances shows a strong correlation with SST, agreeing with previous studies that it is a warm-water indicator.

Acknowledgments

This contribution arose from the doctoral research of JH, which was supported by a Natural Sciences and Engineering Research Council of Canada Discovery grant to MJH. JH publishes with the approval of the Executive Director of the British Geological Survey. IODP is thanked for providing samples. SDS acknowledges funding from The Research Council of Norway (RCN project 229819). We are most grateful to J. Matthiessen and an anonymous reviewer for their helpful comments on the manuscript.

References

Bakken, K., Dale, B., 1986. Dinoflagellate cysts in Upper Quaternary sediments from southwestern Norway and potential correlations with the oceanic record. Boreas 15, 185–190. http://dx.doi.org/10.1111/j.1502-3885.1986.tb00082.x.

Baumann, K.-H., Matthiessen, J., 1992. Variations in surface water mass conditions in the Norwegian Sea: evidence from Holocene coccolith and dinoflagellate cyst assemblages. Mar. Micropaleontol. 20, 129–146. http://dx.doi.org/10.1016/0377-8398(92)90003-3.

Birks, H.J.B., 1995. Quantitative palaeoenvironmental reconstructions. In: Maddy, D., Brew, J.S. (Eds.), Statistical Modelling of Quaternary Science Data. Quaternary Research Association, Cambridge, U.K., pp. 161–254.

Birks, H.J.B., 2003. Quantitative palaeoenvironmental reconstructions from Holocene biological data. In: Mackay, A. (Ed.), Global Change in the Holocene. Arnold, London, pp. 107–123.

Bolton, C.T., Wilson, P.A., Bailey, I., Friedrich, O., Beer, C.J., Becker, J., Baranwal, S., Schiebel, R., 2010. Millennial-scale climate variability in the subpolar North Atlantic Ocean during the late Pliocene. Paleoceanogr. 25, PA4218. http://dx.doi.org/10.1029/2010PA001951.

Broecker, W.S., Peng, T.H., 1988. Tracers in the Sea. Lamont-Doherty Geological Observatory, Palisades, New York, 610pp.

Dale, B., 1976. Cyst formation, sedimentation, and preservation: factors affecting dinoflagellate assemblages in recent sediments from Trondheimsfjord, Norway. Rev. Palaeobot. Palynol. 22, 39–60. http://dx.doi.org/10.1016/0034-6667(76)90010-5.

Dale, B., 1977. New observations on *Peridinium faeroense* Paulsen (1905), and classification of small orthoperidinioid dinoflagellates. British Phycological Journal 12, 241–253.

Dale, B., 1985. Dinoflagellate cyst analysis of Upper Quaternary sediments in core GIK 15530–4 from the Skagerrak. Norsk Geol. Tidsskr. 65, 97–102.

Dale, B., 1996. Dinoflagellate cyst ecology: modeling and geological applications. In: Jansonius, J., McGregor, D.C. (Eds.), Palynology: principles and applications, vol. 3. American Association of Stratigraphic Palynologists Foundation, Dallas, TX, pp. 1249–1275.

Dale, B., 2001. The sedimentary record of dinoflagellate cysts: looking back into the future of phytoplankton blooms. Scientia Marina 65 (suppl. 2), 257–272.

Dale, B., Dale, A.L., 2002. Environmental applications of dinoflagellate cysts and acritarchs. In: Haslett, S.K. (Ed.), Quaternary Environmental Micropalaeontology. Oxford University Press, pp. 207–240.

Dale, B., Fjellså, A., 1994. Dinoflagellate cysts as paleoproductivity indicators: State of the art, potential, and limits. In: Zahn, R., Pedersen, T.F., Kaminski, M.A., Labeyrie, L. (Eds.), Carbon Cycling in the Glacial Ocean: Constraints on the Ocean's Role in Global Change: Quantitative Approaches in Paleoceanography. Springer, Berlin, Heidelberg, pp. 521–537.

Davey, R.J., Rogers, J., 1975. Palynomorph distribution in Recent offshore sediments along two traverses off South West Africa. Mar. Geol. 18, 213–225. http://dx.doi.org/10.1016/0025-3227(75)90097-3.

De Schepper, S., Fischer, E.I., Groeneveld, J., Head, M.J., Matthiessen, J., 2011. Deciphering the palaeoecology of Late Pliocene and Early Pleistocene dinoflagellate cysts. Palaeogeog. Palaeoclimatol. Palaeoecol. 309, 17–32. http://dx.doi.org/10.1016/j.palaeo.2011.04.020.

De Schepper, S., Groeneveld, J., Naafs, B.D.A., Van Renterghem, C., Hennissen, J., Head, M.J., Louwye, S., Fabian, K., 2013. Northern Hemisphere glaciation during the globally warm early Late Pliocene. PLoS ONE 8(12), e81508. http://dx.doi.org/10.1371/journal.pone.0081508.

De Schepper, S., Head, M.J., 2008. Age calibration of dinoflagellate cyst and acritarch events in the Pliocene–Pleistocene of the eastern North Atlantic (DSDP Hole 610A). Stratigraphy 5, 137–161.

De Schepper, S., Head, M.J., Groeneveld, J., 2009. North Atlantic Current variability through marine isotope stage M2 (circa 3.3 Ma) during the mid-Pliocene. Paleoceanogr. 24, PA4206. http://dx.doi.org/10.1029/2008PA001725.

De Schepper, S., Head, M.J., Louwye, S., 2004. New dinoflagellate cyst and incertae sedis taxa from the Pliocene of northern Belgium, southern North Sea Basin. J. Paleontol. 78, 625–644.

de Vernal, A., Eynaud, F., Henry, M., Hillaire-Marcel, C., Londeix, L., Mangin, S., Matthiessen, J., Marret, F., Radi, T., Rochon, A., Solignac, S., Turon, J.L., 2005. Reconstruction of sea-surface conditions at middle to high latitudes of the Northern Hemisphere during the Last Glacial Maximum (LGM) based on dinoflagellate cyst assemblages. Quat. Sci. Rev. 24, 897–924. http://dx.doi.org/10.1016/j.quascirev.2004.06.014.

de Vernal, A., Henry, M., Matthiessen, J., Mudie, P.J., Rochon, A., Boessenkool, K.P., Eynaud, F., Grøsfjeld, K., Guiot, J.L., Hamel, D., Harland, R., Head, M.J., Kunz-Pirrung, M., Levac, E., Loucheur, V., Peyron, O., Pospelova, V., Radi, T., Turon, J.-L., Voronina, E., 2001. Dinoflagellate cyst assemblages as tracers of sea-surface conditions in the northern North Atlantic, Arctic and sub-Arctic seas: the new 'n = 677' data base and its application for quantitative palaeoceanographic reconstruction. J. Quat. Sci. 16, 681–698. http://dx.doi.org/10.1002/jqs.659.

de Vernal, A., Londeix, L., Mudie, P.J., Harland, R., Morzadeck-Kerfourn, M.T., Turon, J.-L., Wrenn, J.H., 1992. Quaternary organic-walled dinoflagellate cysts of the North Atlantic Ocean and adjacent seas: ecostratigraphy and biostratigraphy. In: Head, M.J., Wrenn, J.H. (Eds.), Neogene and Quaternary dinoflagellate cysts and acritarchs. American Association of Stratigraphic Palynologists Foundation, Dallas, TX, pp. 289–328.

de Vernal, A., Mudie, P.J., 1989. Pliocene and Pleistocene palynostratigraphy at ODP Sites 646 and 647, eastern and southern Labrador Sea. Proc. ODP, Sci. Res. 105, 401–422. http://dx.doi.org/10.2973/odp.proc.sr.105.134.1989.

de Vernal, A., Pedersen, T.F., 1997. Micropaleontology and palynology of core PAR87A-10: A 23,000 year record of paleoenvironmental changes in the Gulf of Alaska, northeast North Pacific. Paleoceanogr. 12, 821–830. http://dx.doi.org/10.1029/97pa02167.

de Vernal, A., Rochon, A., Turon, J.-L., Matthiessen, J., 1997. Organic-walled dinoflagellate cysts: Palynological tracers of sea-surface conditions in middle to high latitude marine environments. Geobios 30, 905–920. http://dx.doi.org/10.1016/S0016-6995(97)80215-X.

818 de Vernal, A., Turon, J.-L., Guiot, J., 1994. Dinoflagellate cyst distribution in high-latitude
819 marine environments and quantitative reconstruction of sea-surface salinity, temperature, and
820 seasonality. Can. J. Earth Sci. 31, 48–62. http://dx.doi.org/10.1139/e94-006.

821 Devillers, R., de Vernal, A., 2000. Distribution of dinoflagellate cysts in surface sediments of the
822 northern North Atlantic in relation to nutrient content and productivity in surface waters. Mar.
823 Geol. 166, 103–124. http://dx.doi.org/10.1016/S0025-3227(00)00007-4.

824 Dodge, J.D., Harland, R., 1991. The distribution of planktonic dinoflagellates and their cysts in
825 the eastern and northeastern Atlantic Ocean. New Phytologist 118, 593–603.
826 http://dx.doi.org/10.1111/j.1469-8137.1991.tb01000.x

827 Dowling, L., McCave, I.N., 1993. Sedimentation on the Feni Drift and Late Glacial bottom water
828 production in the northern Rockall Trough. Sediment. Geol. 82, 79–87.
829 http://dx.doi.org/10.1016/0037-0738(93)90114-K.

830 Edwards, L.E., Mudie, P.J., de Vernal, A., 1991. Pliocene paleoclimatic reconstruction using
831 dinoflagellate cysts: Comparison of methods. Quat. Sci. Rev. 10, 259–274.
832 http://dx.doi.org/10.1016/0277-3791(91)90024-O.

833 Expedition 306 Scientists, 2006. Expedition 306 summary. Proc. IODP 303/306, 1–29.
834 http://dx.doi.org/10.2204/iodp.proc.303306.109.2006.

835 Eynaud, F., Turon, J.L., Duprat, J., 2004. Comparison of the Holocene and Eemian
836 palaeoenvironments in the South Icelandic Basin: dinoflagellate cysts as proxies for the North
837 Atlantic surface circulation. Rev. Palaeobot. Palyno. 128, 55–79.
838 http://dx.doi.org/10.1016/S0034-6667(03)00112-X.

839 Eynaud, F., Turon, J.L., Sanchez-Goni, M., Gendreau, S., 2000. Dinoflagellate cyst evidence of
840 'Heinrich-like events'; off Portugal during the Marine Isotopic Stage 5. Mar. Micropaleontol. 40,
841 9–21. http://dx.doi.org/ 10.1016/S0377-8398(99)00045-6.

842 Friedrich, O., Wilson, P.A., Bolton, C.T., Beer, C.J., Schiebel, R., 2013. Late Pliocene to early
843 Pleistocene changes in the North Atlantic Current and suborbital-scale sea-surface temperature
844 variability. Paleoceanogr. 28, 274–282. http://dx.doi.org/10.1002/palo.20029.

845 Harland, R., 1973. Quaternary (Flandrian?) dinoflagellate cysts from the Grand Banks, off
846 Newfoundland, Canada. Rev. Palaeobot. Palyno. 16, 229–242. http://dx.doi.org/10.1016/0034-
847 6667(73)90021-3.

848 Harland, R., 1979. Dinoflagellate biostratigraphy of Neogene and Quaternary sediments at Holes
849 400/400A in the Bay of Biscay (Deep Sea Drilling Project Leg 48). Proc. DSDP, Init. Rep. 48,
850 531–545. http://dx.doi.org/10.2973/dsdp.proc.48.122.1979.

851 Harland, R., 1983. Distribution maps of Recent dinoflagellate cysts in bottom sediments from the
852 North Atlantic Ocean and adjacent seas. Palaeontology 26, 321–387.

853 Harland, R., 1984. Recent and Late Quaternary dinoflagellate cysts from the area of the
854 Greenland–Iceland–Faeroe–Scotland Ridge. J. Micropalaeontol. 3, 95–108.
855 http://dx.doi.org/10.1144/jm.3.2.95.

856 Harland, R., Pudsey, C.J., 1999. Dinoflagellate cysts from sediment traps deployed in the
857 Bellingshausen, Weddell and Scotia seas, Antarctica. Mar. Micropaleontol. 37, 77–99.
858 http://dx.doi.org/10.1016/S0377-8398(99)00016-X.

859 Head, M.J., 1994. Morphology and paleoenvironmental significance of the Cenozoic
860 dinoflagellate genera *Tectatodinium* and *Habibacysta*. Micropaleontology 40, 289–321.
861 http://dx.doi.org/10.2307/1485937.

862 Head, M.J., 1996. Late Cenozoic dinoflagellates from the Royal Society borehole at Ludham,
863 Norfolk, eastern England. J. Paleontol. 70, 543–570.

864 Head, M.J., Edwards, L.E., Garrett, J.K., Lentin, J.K., Marret, F., Matsuoka, K., Matthiessen, J.,
865 O'Mahony, J., Sun, X., de Verteuil, L., Zevenboom, D., 1993. A forum on Neogene and
866 Quaternary dinoflagellate cysts: The edited transcript of a round table discussion held at the Third
867 Workshop on Neogene and Quaternary Dinoflagellates; with taxonomic appendix. Palynology 17,
868 201–239. http://dx.doi.org/10.1080/01916122.1993.9989428.

869 Head, M.J., Norris, D., Mudie, P., 1989a. New species of dinocysts and a new species of acritarch
870 from the upper Miocene and lowermost Pliocene, ODP Leg 105, site 646, Labrador Sea. Proc.
871 ODP, Sci. Res. 105, 453–466. http://dx.doi.org/10.2973/odp.proc.sr.105.136.1989.

872 Head, M.J., Norris, G., Mudie, P.J., 1989b. Palynology and dinocyst stratigraphy of the Miocene
873 in ODP Leg 105, Hole 645E, Baffin Bay. Proc. ODP, Sci. Res. 105, 467–514.
874 http://dx.doi.org/10.2973/odp.proc.sr.105.137.1989.

875 Head, M.J., Norris, G., Mudie, P.J., 1989c. Palynology and dinocyst stratigraphy of the upper
876 Miocene and lowermost Pliocene, ODP Leg 105, Site 646, Labrador Sea. Proc. ODP, Sci. Res.
877 105, 423–451. http://dx.doi.org/10.2973/odp.proc.sr.105.135.1989.

878 Head, M.J., Riding, J. B., Eidvin, T., Chadwick, R. A., 2004. Palynological and foraminiferal
879 biostratigraphy of (Upper Pliocene) Nordland Group mudstones at Sleipner, northern North Sea.
880 Mar. Pet. Geol. 21, 277–297. http://dx.doi.org/10.1016/j.marpetgeo.2003.12.002.

881 Hennissen, J.A.I., Head, M.J., De Schepper, S., Groeneveld, J., 2014. Palynological evidence for
882 a southward shift of the North Atlantic Current at ~2.6 Ma during the intensification of late
883 Cenozoic Northern Hemisphere glaciation. Paleoceanogr. 29, 564–580.
884 http://dx.doi.org/10.1002/2013pa002543.

885 Hennissen, J.A.I., Head, M.J., De Schepper, S., Groeneveld, J., 2015. Increased seasonality
886 during the intensification of Northern Hemisphere glaciation at the Pliocene–Pleistocene
887 transition ~2.6 Ma. Quat. Sci. Rev. 129, 321–332.
888 http://dx.doi.org/10.1016/j.quascirev.2015.10.010.

889 Hill, M.O., Gauch, H.G., Jr., 1980. Detrended correspondence analysis: An improved ordination
890 technique. Vegetatio 42, 47–58. http://dx.doi.org/10.1007/bf00048870.

891 Hutchinson, G.E., 1957. Concluding remarks. Cold Spring Harbor Symposia on Quantitative
892 Biology 22, 415–427. http://dx.doi.org/10.1101/sqb.1957.022.01.039.

893 Imbrie, J., Kipp, N.G., 1971. A new micropaleontological method for quantitative
894 paleoclimatology: application to a late Pleistocene Caribbean core. In: Turekian, K. (Ed.), The
895 Late Cenozoic Ice Ages. Yale University Press, New Haven, pp. 71–181.

Jansson, I.-M., Mertens, K.N., and Head, M.J. with contributions from de Vernal, A., Londeix, L., Marret, F., Matthiessen, J., and Sangiorgi, F., 2014. Statistically assessing the correlation between salinity and morphology in cysts produced by the dinoflagellate *Protoceratium reticulatum* from surface sediments of the North Atlantic Ocean, Mediterranean–Marmara–Black Sea region, and Baltic–Kattegat–Skagerrak estuarine system. Palaeogeog., Palaeoclimatol., Palaeoecol. 399, 202–213.

Kleiven, H.F., Jansen, E., Fronval, T., Smith, T., 2002. Intensification of Northern Hemisphere glaciations in the circum Atlantic region (3.5–2.4 Ma) – ice-rafted detritus evidence. Palaeogeog. Palaeoclimatol. Palaeoecol. 184, 213–223. http://dx.doi.org/10.1016/S0031-0182(01)00407-2.

Leps, J., Smilauer, P., 2003. Multivariate Analysis of Ecological Data using CANOCO. Cambridge University Press, Cambridge, UK, pp. 283.

Lisiecki, L.E., Raymo, M.E., 2005. A Pliocene-Pleistocene stack of 57 globally distributed benthic $\delta^{18}O$ records. Paleoceanogr. 20. http://dx.doi.org/10.1029/2004PA001071.

Locarnini, R., Mishonov, A., Antonov, J., Boyer, T., Garcia, H., Baranova, O., Zweng, M., Paver, C., Reagan, J., Johnson, D., Hamilton, M., Seidov, D., 2013. World Ocean Atlas 2013, Volume 1: Temperature, in: Levitus, S., Mishonov, A. (Eds.), NOAA Atlas Nesdis 73, pp. 1–40.

Louwye, S., Head, M.J., De Schepper, S., 2004. Dinoflagellate cyst stratigraphy and palaeoecology of the Pliocene in northern Belgium, southern North Sea Basin. Geol. Mag. 141, 353–378. https://doi.org/10.1017/S0016756804009136.

Marret, F., de Vernal, A., 1997. Dinoflagellate cyst distribution in surface sediments of the southern Indian Ocean. Mar. Micropaleontol. 29, 367–392. http://dx.doi.org/10.1016/S0377-8398(96)00049-7.

Matthiessen, J., 1995. Distribution patterns of dinoflagellate cysts and other organic-walled microfossils in recent Norwegian–Greenland Sea sediments. Mar. Micropaleontol. 24, 307–334. http://dx.doi.org/10.1016/0377-8398(94)00016-G.

Matthiessen, J., Knies, J., 2001. Dinoflagellate cyst evidence for warm interglacial conditions at the northern Barents Sea margin during marine oxygen isotope stage 5. J. Quat. Sci. 16, 727–737. http://dx.doi.org/10.1002/jqs.656.

Matthiessen, J., de Vernal, A., Head, M., Okolodkov, Y., Zonneveld, K., Harland, R. 2005. Modern organic-walled dinoflagellate cysts in Arctic marine environments and their (paleo-) environmental significance. Paläontologische Zeitschrift 79, 3–51.

Mertens, K.N., Ribeiro, S., Bouimetarhan, I., Caner, H., Combourieu Nebout, N., Dale, B., de Vernal, A., Ellegaard, M., Filipova, M., Godhe, A., 2009. Process length variation in cysts of a dinoflagellate, *Lingulodinium machaerophorum*, in surface sediments: investigating its potential as salinity proxy. Mar. Micropaleontol. 70, 54–69. http://dx.doi.org/10.1016/j.marmicro.2008.10.004.

Mudie, P.J., 1992. Circum-arctic Quaternary and Neogene marine palynofloras: paleoecology and statistical analysis. In: Head, M.J., Wrenn, J.H. (Eds.), Neogene and Quaternary Dinoflagellate Cysts and Acritarchs. American Association of Stratigraphic Palynologists Foundation, Dallas, TX, pp. 347–390.

936 Mudie, P.J., 1996. Pellets of dinoflagellate-eating zooplankton. In: Jansonius, J., McGregor, D.C.
937 (Eds.), Palynology: principles and applications, vol. 3. American Association of Stratigraphic
938 Palynologists Foundation, Dallas, TX, pp. 1087–1089.

939 Naafs, B.D.A., Stein, R., Hefter, J., Khélifi, N., De Schepper, S., Haug, G.H., 2010. Late Pliocene
940 changes in the North Atlantic Current. Earth Planet. Sci. Lett. 298, 434–442.
941 http://dx.doi.org/10.1016/j.epsl.2010.08.023.

942 Naafs, B.D.A., Hefter, J., Stein, R., 2013. Millennial-scale ice rafting events and Hudson Strait
943 Heinrich(-like) Events during the late Pliocene and Pleistocene: a review. Quat. Sci. Rev. 80, 1-
944 28. http://dx.doi.org/10.1016/j.quascirev.2013.08.014.

945 Oksanen, J., Blanchet, F.G., Kindt, R., Legendre, P., Minchin, P.R., O'Hara, R.B., Simpson,
946 G.L., Solymos, P., Stevens, M.H.H., Wagner, H., 2013. Vegan: Community Ecology Package, R
947 package version 2.0-6 ed.

948 Paez-Reyes, M., Head, M.J., 2013. The Cenozoic gonyaulacacean dinoflagellate genera
949 *Operculodinium* Wall, 1967 and *Protoceratium* Bergh, 1881 and their phylogenetic relationships.
950 J. Paleontol. 87, 786–803. http://dx.doi.org/10.1666/12-103.

951 Pelegrí, J.L., Csanady, G.T., Martins, A., 1996. The North Atlantic nutrient stream. J. Oceanogr.
952 52, 275–299. http://dx.doi.org/10.1007/bf02235924.

953 Penaud, A., Eynaud, F., Turon, J.L., Zaragosi, S., Marret, F., Bourillet, J.F., 2008. Interglacial
954 variability (MIS 5 and MIS 7) and dinoflagellate cyst assemblages in the Bay of Biscay (North
955 Atlantic). Mar. Micropaleontol. 68, 136–155. http://dx.doi.org/10.1016/j.marmicro.2008.01.007.

956 R Core Team., 2013. A language and environment for statistical computing. R Foundation for
957 Statistical Computing, Vienna, Austria.

958 Radi, T., de Vernal, A., 2008. Dinocysts as proxy of primary productivity in mid–high latitudes of
959 the Northern Hemisphere. Mar. Micropaleontol. 68, 84–114.
960 http://dx.doi.org/10.1016/j.marmicro.2008.01.012.

961 Rintoul, S.R., Wunsch, C., 1991. Mass, heat, oxygen and nutrient fluxes and budgets in the North
962 Atlantic Ocean. Deep Sea Res. 38, S355–S377. http://dx.doi.org/10.1016/S0198-0149(12)80017-
963 3.

964 Rochon, A., de Vernal, A., Turon, J.-L., Matthiessen, J., Head, M.J., 1999. Distribution of recent
965 dinoflagellate cysts in surface sediments from the North Atlantic Ocean and adjacent seas in
966 relation to sea-surface parameters. AASP Contrib. Ser. 35, pp. 1–152.

967 Sarnthein, M., Winn, K., Duplessy, J.-C., Fontugne, M.R., 1988. Global variations of surface
968 ocean productivity in low and mid latitudes: Influence on CO2 reservoirs of the deep ocean and
969 atmosphere during the last 21,000 years. Paleoceanogr. 3, 361–399.
970 http://10.1029/PA003i003p00361.

971 Sildever, S., Joest Andersen, T., Ribeiro, S., Ellegaard, M., 2015. Influence of surface salinity
972 gradient on dinoflagellate cyst community structure, abundance and morphology in the Baltic
973 Sea, Kattegat and Skagerrak: Estuarine, Coastal and Shelf Science 155, 1–7,
974 http://dx.doi.org/10.1016/j.ecss.2015.01.003.

975 Stockmarr, J., 1971. Tablets with spores used in absolute pollen analysis. Pollen et spores 13,
976 615–621.

977 Stoker, M.S., Praeg, D., Hjelstuen, B.O., Laberg, J.S., Nielsen, T., Shannon, P.M., 2005. Neogene
978 stratigraphy and the sedimentary and oceanographic development of the NW European Atlantic
979 margin. Mar. Pet. Geol. 22, 977–1005. http://dx.doi.org/10.1016/j.marpetgeo.2004.11.007.

980 Swift, J.H., Aagaard, K., 1981. Seasonal transitions and water mass formation in the Iceland and
981 Greenland seas. Deep Sea Research Part A. Oceanographic Research Papers 28, 1107–1129.
982 http://10.1016/0198-0149(81)90050-9.

983 Telford, R.J., 2006. Limitations of dinoflagellate cyst transfer functions. Quat. Sci. Rev. 25,
984 1375–1382. http://dx.doi.org/10.1016/j.quascirev.2006.02.012.

985 Telford, R.J., Birks, H.J.B., 2009. Evaluation of transfer functions in spatially structured
986 environments. Quat. Sci. Rev. 28, 1309–1316. http://dx.doi.org/10.1016/j.quascirev.2008.12.020.

987 Telford, R.J., Birks, H.J.B., 2011. QSR Correspondence "Is spatial autocorrelation introducing
988 biases in the apparent accuracy of palaeoclimatic reconstructions?". Quat. Sci. Rev. 30, 3210–
989 3213. http://dx.doi.org/10.1016/j.quascirev.2011.07.019.

990 ter Braak, C.J.F., 1985. Correspondence analysis of incidence and abundance data: Properties in
991 terms of a unimodal response model. Biometrics 41, 859–873. http://dx.doi.org/10.2307/2530959.

992 ter Braak, C.J.F., 1986. Canonical correspondence analysis: a new eigenvector technique for
993 multivariate direct gradient analysis. Ecology 67, 1167–1179. http://dx.doi.org/10.2307/1938672.

994 ter Braak, C.J.F., Prentice, I.C., 1988. A theory of gradient analysis. Advances in Ecological
995 Research 18, 271–317. http://dx.doi.org/10.1016/S0065-2504(08)60183-X.

996 Turon, J.-L., Londeix, L., 1988. Les assemblages de kystes de dinoflagellés en Méditerranée
997 occidentale (Mer d'Alboran). Mise en évidence de l'évolution des paléoenvironnements depuis le
998 dernier maximum glaciaire. Bulletin des centres de recherches Exploration-production Elf-
999 Aquitaine 12, 313–344.

1000 Udeze, C.U., Oboh-Ikuenobe, F.E., 2005. Neogene palaeoceanographic and palaeoclimatic events
1001 inferred from palynological data: Cape Basin off South Africa, ODP Leg 175. Palaeogeog.
1002 Palaeoclimatol. Palaeoecol. 219, 199–223. http://dx.doi.org/10.1016/j.palaeo.2004.12.026.

1003 Versteegh, G.J.M., 1994. Recognition of cyclic and non-cyclic environmental changes in the
1004 Mediterranean Pliocene: A palynological approach. Mar. Micropaleontol. 23, 147–183.
1005 http://dx.doi.org/10.1016/0377-8398(94)90005-1.

1006 Versteegh, G.J.M., 1997. The onset of major Northern Hemisphere glaciations and their impact
1007 on dinoflagellate cysts and acritarchs from the Singa section, Calabria (southern Italy) and DSDP
1008 Holes 607/607A (North Atlantic). Mar. Micropaleontol. 30, 319–343.
1009 http://dx.doi.org/10.1016/S0377-8398(96)00052-7.

1010 Versteegh, G.J.M., Brinkhuis, H., Visscher, H., Zonneveld, K.A.F., 1996. The relation between
1011 productivity and temperature in the Pliocene North Atlantic at the onset of northern hemisphere
1012 glaciation: a palynological study. Global Planet. Change 11, 155–165.
1013 http://dx.doi.org/10.1016/0921-8181(95)00054-2.

1014 Versteegh, G.J.M., Zonneveld, K.A.F., 1994. Determination of (palaeo-)ecological preferences of
1015 dinoflagellates by applying Detrended and Canonical Correspondence analysis to Late Pliocene
1016 dinoflagellate cyst assemblages of the south Italian Singa section. Rev. Palaeobot. Palyno. 84,
1017 181–199. http://dx.doi.org/10.1016/0034-6667(94)90050-7.

1018 Wall, D., Dale, B., 1966. "Living Fossils" in Western Atlantic Plankton. Nature 211, 1025–1026
1019 http://dx.doi.org/10.1038/2111025a0.

1020 Wall, D., Dale, B., Lohmann, G.P., Smith, W.K., 1977. The environmental and climatic
1021 distribution of dinoflagellate cysts in modern marine sediments from regions in the North and
1022 South Atlantic Oceans and adjacent seas. Mar. Micropaleontol. 2, 121–200.
1023 http://dx.doi.org/10.1016/0377-8398(77)90008-1.

1024 Warny, S., Askin, R.A., Hannah, M.J., Mohr, B.A.R., Raine, J.I., Harwood, D.M., Florindo, F.,
1025 SMS Science Team, 2009. Palynomorphs from a sediment core reveal a sudden remarkably warm
1026 Antarctica during the middle Miocene. Geology 37, 955–958.
1027 http://dx.doi.org/10.1130/G30139A.1.

1028 Whittaker, R.H., 1967. Gradient analysis of vegetation. Biological Reviews 42, 207–264.
1029 http://dx.doi.org/10.1111/j.1469-185X.1967.tb01419.x.

1030 Williams, D.B., 1971. The occurrence of dinoflagellates in marine sediments. In: Funnell, B.M.,
1031 Riedel, W.R. (Eds.), The Micropalaeontology of Oceans. Cambridge University Press,
1032 Cambridge, U.K., pp. 231–244.

1033 Zahn, R., Winn, K., Sarnthein, M., 1986. Benthic foraminiferal $\delta^{13}C$ and accumulation rates of
1034 organic carbon: *Uvigerina peregrina* group and *Cibicidoides wuellerstorfi*. Paleoceanogr. 1, 27–
1035 42. http://10.1029/PA001i001p00027.

1036 Zonneveld, K.A.F., Marret, F., Versteegh, G.J.M., Bogus, K., Bonnet, S., Bouimetarhan, I.,
1037 Crouch, E., de Vernal, A., Elshanawany, R., Edwards, L., Esper, O., Forke, S., Grøsfjeld, K.,
1038 Henry, M., Holzwarth, U., Kielt, J.-F., Kim, S.-Y., Ladouceur, S., Ledu, D., Chen, L., Limoges,
1039 A., Londeix, L., Lu, S.H., Mahmoud, M.S., Marino, G., Matsouka, K., Matthiessen, J.,
1040 Mildenhal, D.C., Mudie, P., Neil, H.L., Pospelova, V., Qi, Y., Radi, T., Richerol, T., Rochon, A.,
1041 Sangiorgi, F., Solignac, S., Turon, J.-L., Verleye, T., Wang, Y., Wang, Z., Young, M., 2013.
1042 Atlas of modern dinoflagellate cyst distribution based on 2405 data points. Rev. Palaeobot.
1043 Palynol. 191, 1–197. http://dx.doi.org/10.1016/j.revpalbo.2012.08.003.

1044

1045 Figure 1: Location of the studied sites IODP U1313 and DSDP 610 and other DSDP/ODP/IODP Sites
1046 where the Pliocene–Pleistocene boundary time slab has been cored.

1047 Figure 2: Abundance/concentration signatures of selected dinoflagellate cysts (a–l) and synoptic
1048 diagram of dinocyst assemblage compositions (m) in DSDP Hole 610A. Species abbreviations as in
1049 Table 1. The grey columns indicate even-numbered ("cold") marine isotope stages.

1050 Figure 3: Abundance/concentration signatures of selected dinoflagellate cysts (a–m) and synoptic
1051 diagram of dinocyst assemblage compositions (n) in DSDP Hole U1313C. Species abbreviations as in
1052 Table 1. The light grey bars indicate even-numbered ("cold") marine isotope stages.

1053 Figure 4: Detrended correspondence analysis (DCA) of the samples (open orange circles, see also Fig.
1054 5) and species (black) in DSDP Hole 610A. Species abbreviations as in Table 1. Species in bold
1055 represent species with statistical weights in the upper quartile.

1056 Figure 5: Detrended correspondence analysis (DCA) of the samples in DSDP Hole 610A. Samples
1057 with a relative abundance of *O. centrocarpum* exceeding 60% are shown in red; samples with a
1058 relative abundance of *O. centrocarpum* less than 10% are shown in blue; remaining samples are
1059 shown in black.

1060 Figure 6: Correspondence analysis (CA) of the samples (open orange circles) and species (black) in
1061 IODP Hole U1313C. Species abbreviations as in Table 1. Species in bold represent species with
1062 statistical weights in the upper quartile.

1063 Figure 7: Correspondence analysis (CA) of the samples in IODP Hole U1313C. Samples containing
1064 *Invertocysta lacrymosa* are shown in red; samples with a relative abundance of the *Spiniferites*
1065 *mirabilis* group that exceeds 10% are shown in blue; remaining samples are shown in black.

1066 Figure 8: Canonical correspondence analysis (CCA) for samples (open orange circles) and species
1067 (black) in DSDP Hole 610A, with $\delta^{18}O_{bul}$, SST, $\delta^{18}O_{sal}$, dinoflagellate cyst burial flux (DBF), age,

1068 IN/O, and ON/O as constraining factors. Species abbreviations follow Table 1. Upper quartile species
1069 in DCA are shown in bold.

1070 Figure 9: Canonical correspondence analysis (CCA) of the samples in DSDP Hole 610A. Constraining
1071 factors as in Figure 8.

1072 Figure 10: Canonical correspondence analysis (CCA) for samples (open orange circles) and species
1073 (black) in IODP Hole U1313C, with $\delta^{18}O_{bul}$, SST, $\delta^{18}O_{sal}$, dinoflagellate cyst burial flux (DBF), age,
1074 IN/O, ON/O, and seasonality as constraining factors. Species abbreviations as in Table 1. Upper
1075 quartile species in DCA are shown in bold.

1076 Figure 11: Canonical correspondence analysis (CCA) in IODP Hole U1313C, showing the samples
1077 only. Constraining factors as in Figure 10.

1078 Figure 12: Geochemical, palynological, and IRD results for DSDP Hole 610A and IODP Hole
1079 U1313C across the Pliocene–Pleistocene boundary. Marine isotope stages (grey columns indicating
1080 glacials) follow Lisiecki and Raymo (2005). a: Seasonality ($SST_{rub-bul}$) record from Hole U1313C
1081 (black) with average values before and after MIS 104 indicated in grey (Hennissen et al., 2015) and
1082 present day seasonality (dashed line; Locarnini et al., 2013), IRD (orange; Kleiven et al., 2002) and
1083 $\delta^{18}O_{sal}$ (red; Hennissen et al., 2014) for Hole 610A; b: Dinocyst concentration (red) and dinocyst
1084 burial flux (black) for Hole 610A (Hennissen et al., 2014) and $\delta^{13}C_{bul}$ (blue) for Hole 610A; c:
1085 Seasonality ($SST_{rub-bul}$) record for Hole U1313C (black) with average values before and after MIS 104
1086 indicated in grey and present day seasonality (dashed line) based on Locarnini et al. (2013),
1087 quartz/calcite as an IRD indicator for Hole U1313C (orange; Naafs et al., 2013) and $\delta^{18}O_{sal}$ (red;
1088 Hennissen et al., 2014); d: Dinocyst concentration (red) and dinocyst burial flux (black) for Hole
1089 U1313C (Hennissen et al., 2014) and $\delta^{13}C_{bul}$ (blue) for Hole U1313C.

1090 Figure 13: a: SST based on *G. bulloides* in Hole 610A (red) and U1313C (black) (Hennissen et al.,
1091 2014); b: $\delta^{18}O_{bul}$ in Hole 610A (red) and U1313C (black); c: Seasonality in Hole U1313C (Hennissen

et al., 2015); d: DCA values of the first two axes in Hole 610A; e: CA values of the first two axes in Hole U1313C.

Figure 14: Sea surface temperature (SST) ranges of species with statistical weights in the highest quartile in DSDP Hole 610A. Relative abundances (y axis) are compared to SST (x axis) and $\delta^{18}O_{sal}$ (colour of the marker).

Figure 15: Sea surface temperature (SST) ranges of species with statistical weights in the highest quartile in DSDP Hole 610A. Relative abundances (y axis) are compared to SST (x axis) and $\delta^{18}O_{sal}$ (color of the marker). Species abbreviations as in Table 1.

Figure 16: Sea surface temperature (SST) ranges of species with statistical weights in the highest quartile in IODP Hole U1313C. Relative abundances (y axis) are compared to SST (x axis) and $\delta^{18}O_{bul}$ (color of the marker). Species abbreviations as in Table 1.

Table 1: Codes for species employed in the statistical analysis in the current study.

Table 2: Species used to calculate the inner neritic/oceanic (IN/O) and outer neritic/oceanic (ON/O) ratios.

Table 3: Detrended correspondence analysis (DCA) of the studied interval in DSDP Hole 610A: eigenvalues and species scores for the first four axes. Axes DCA1–DCA2 are shown in Figure 6. Species with a statistical weight, a reflection of its influence on sample distribution in DCA, in the highest quartile are indicated in bold. Species with high statistical weights and high scores on axes with high eigenvalues are indicator species whereas species having a high statistical weight and low scores on axes with high eigenvalues are cosmopolitan (Dale and Dale, 2002).

Table 4: Correspondence analysis (CA) of the studied interval in IODP Hole U1313C: eigenvalues and species scores for the first four axes. Axes CA1–CA2 are shown in Figure 7. Species with a

statistical weight, a reflection of its influence on sample distribution in DCA, in the highest quartile are indicated in bold. Species with high statistical weights and high scores on axes with high eigenvalues are indicator species whereas species having a high statistical weight and low scores on axes with high eigenvalues are cosmopolitan (Dale and Dale, 2002).

Table 5: Eigenvalues of the first four axes of (detrended) correspondence analysis (D)CA and (detrended) canonical correspondence analysis (D)CCA in DSDP Hole 610A and IODP Hole U1313C.

Table 6: Summary of extant species and their Plio-Pleistocene SST ranges in DSDP Hole 610A and IODP Hole U1313C and modern distributions. Note that the full ranges of sea-surface temperatures (SSTs) reconstructed for Holes 610A and U1313 in this study are 8–16°C and 12–23°C respectively.

Table 7: Summary of extinct species and their Plio-Pleistocene SST ranges in DSDP Hole 610A and IODP Hole U1313C. Note that the full ranges of sea-surface temperatures (SSTs) reconstructed for Holes 610A and U1313 in this study are 8–16°C and 12–23°C respectively.

Table 1: Codes for species employed in the statistical analysis in the current study.

Table 2: Species used to calculate the inner neritic/oceanic (IN/O) and outer neritic/oceanic (ON/O) ratios.

Table 3: Detrended correspondence analysis (DCA) of the studied interval in DSDP Hole 610A: eigenvalues and species scores for the first four axes. Axes DCA1–DCA2 are shown in Figure 6. Species with a statistical weight, a reflection of its influence on sample distribution in DCA, in the highest quartile are indicated in bold. Species with high statistical weights and high scores on axes with high eigenvalues are indicator species whereas species having a high statistical weight and low scores on axes with high eigenvalues are cosmopolitan (Dale and Dale, 2002).

Table 4: Correspondence analysis (CA) of the studied interval in IODP Hole U1313C: eigenvalues and species scores for the first four axes. Axes CA1–CA2 are shown in Figure 7. Species with a statistical weight, a reflection of its influence on sample distribution in DCA, in the highest quartile are indicated in bold. Species with high statistical weights and high scores on axes with high eigenvalues are indicator species whereas species having a high statistical weight and low scores on axes with high eigenvalues are cosmopolitan (Dale and Dale, 2002).

Table 5: Eigenvalues of the first four axes of (detrended) correspondence analysis (D)CA and (detrended) canonical correspondence analysis (D)CCA in DSDP Hole 610A and IODP Hole U1313C.

Table 6: Summary of extant species and their Plio-Pleistocene SST ranges in DSDP Hole 610A and IODP Hole U1313C and modern distributions. Note that the full ranges of sea-surface temperatures (SSTs) reconstructed for Holes 610A and U1313 in this study are 8–16°C and 12–23°C respectively.

Table 7: Summary of extinct species and their Plio-Pleistocene SST ranges in DSDP Hole 610A and IODP Hole U1313C. Note that the full ranges of sea-surface temperatures (SSTs) reconstructed for Holes 610A and U1313 in this study are 8–16°C and 12–23°C respectively.

1154 Figures

1155

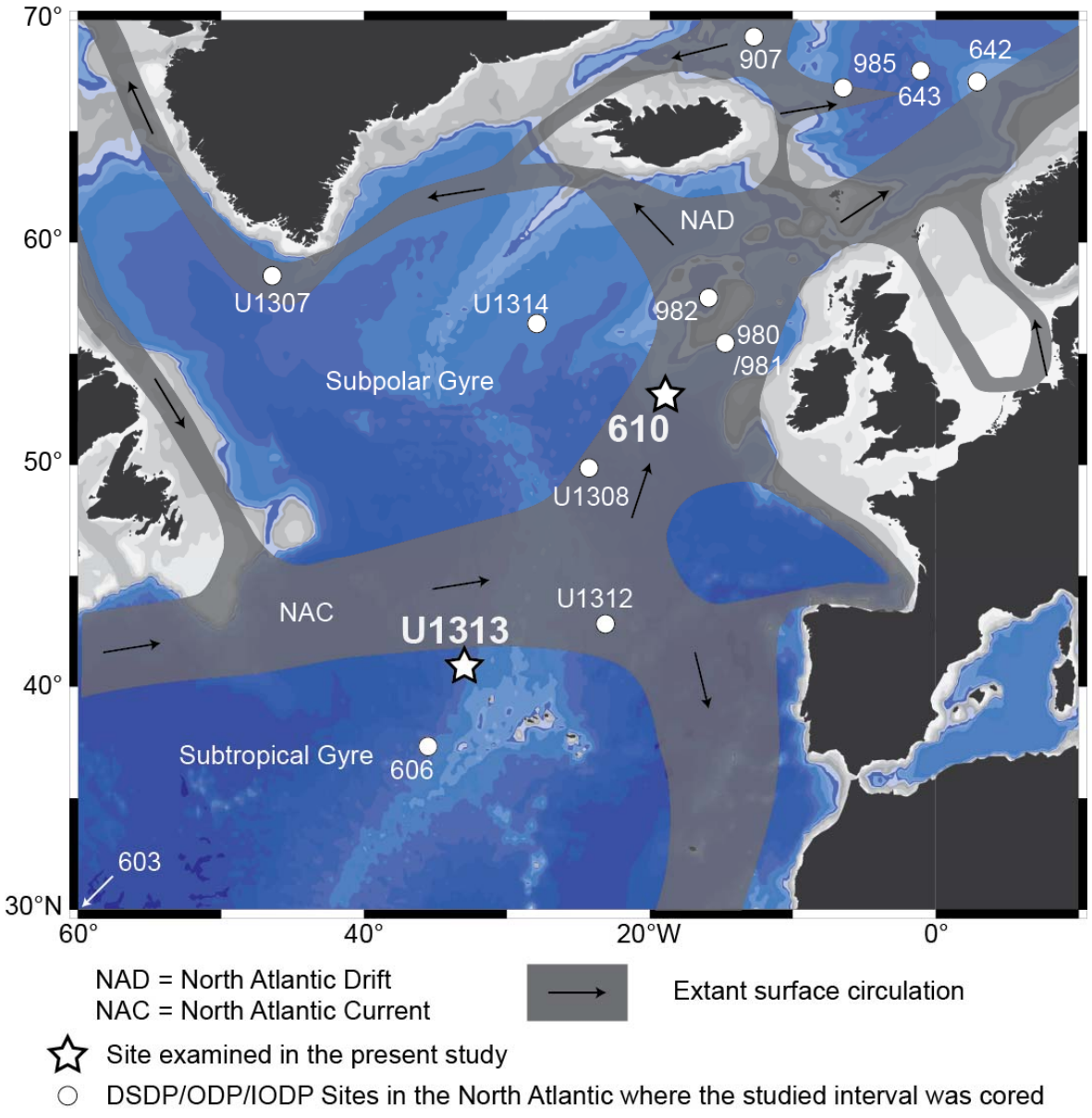

1156

1157 Figure 1

1158

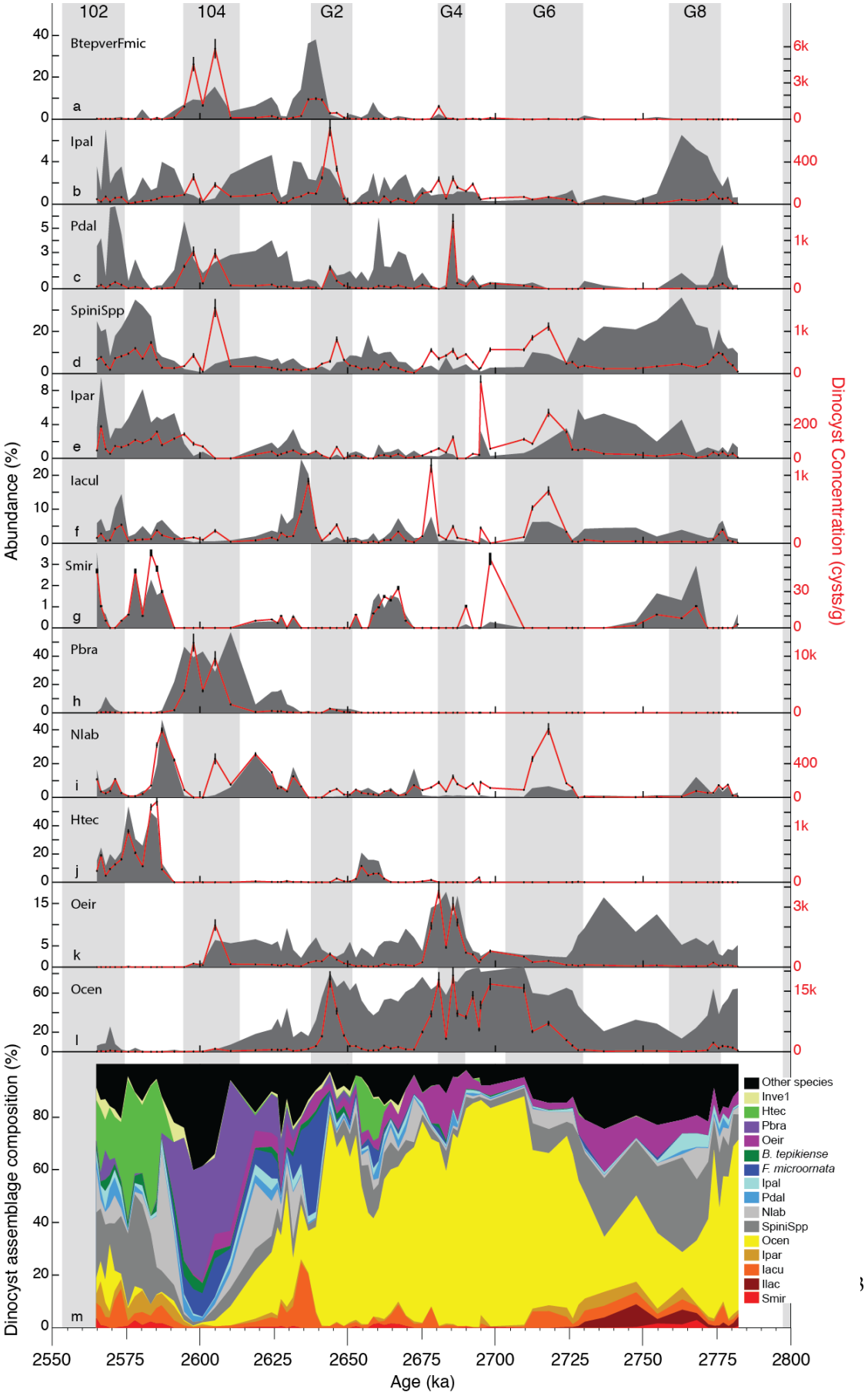
102
104
G2
G4
G6
G8
BtepverFmic
a
Ipal
b
Pdal
c
SpiniSpp
d
Ipar
e
Iacul
f
Smir
g
Pbra
h
Nlab
i
Htec
j
Oeir
k
Ocen
l
m
Abundance (%)
Dinocyst Concentration (cysts/g)
Dinocyst assemblage composition (%)
Age (ka)
2550
2575
2600
2625
2650
2675
2700
2725
2750
2775
2800
Other species
Inve1
Htec
Pbra
Oeir
B. tepikiense
F. microornata
Ipal
Pdal
Nlab
SpiniSpp
Ocen
Ipar
Iacu
Ilac
Smir

1160 Fig 2

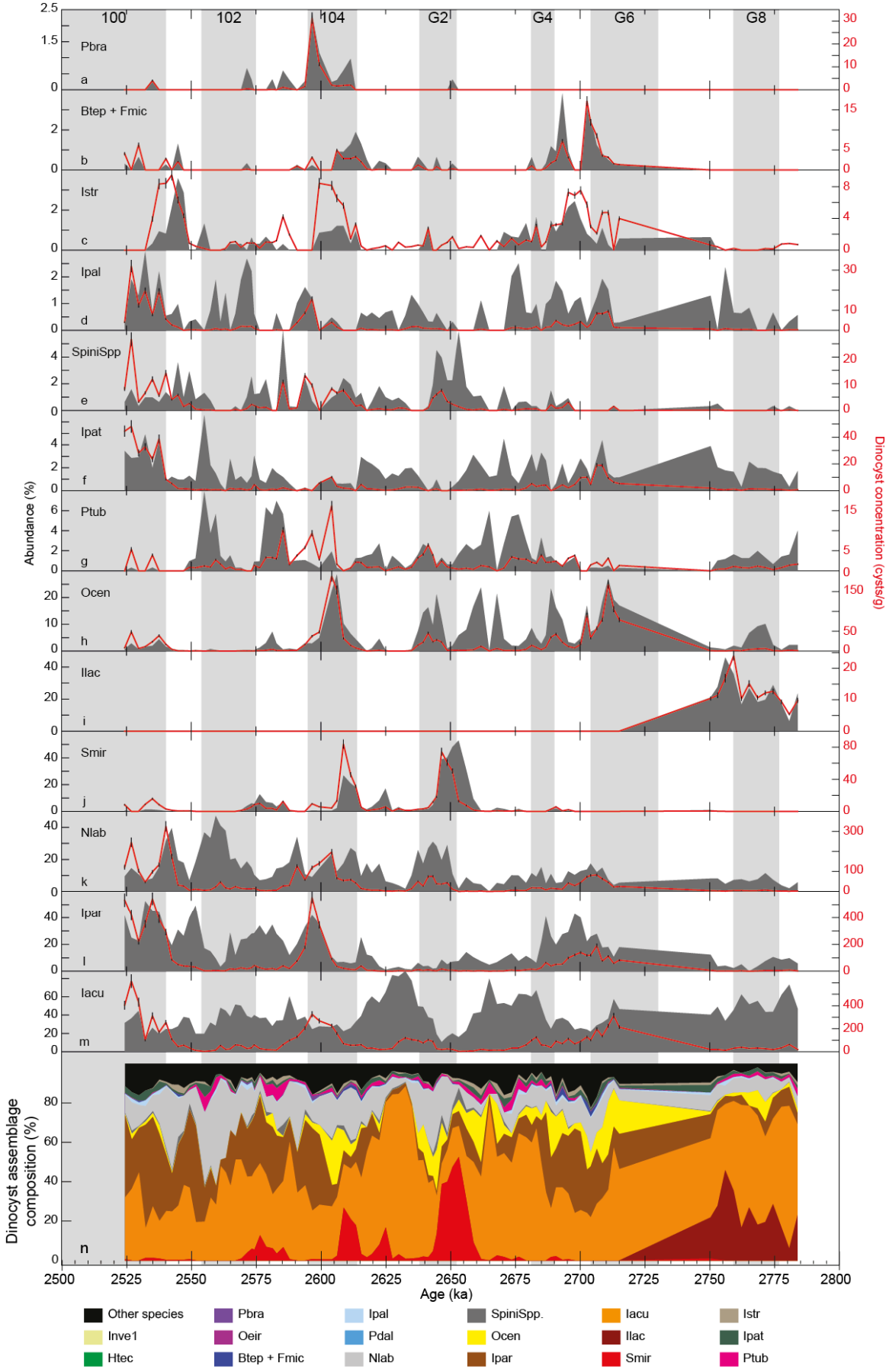
100
102
104
G2
G4
G6
G8
Pbra
a
Btep + Fmic
b
Istr
c
Ipal
d
SpiniSpp
e
Ipat
f
Ptub
g
Ocen
h
Ilac
i
Smir
j
Nlab
k
Ipar
l
Iacu
m
n
Abundance (%)
Dinocyst concentration (cysts/g)
Dinocyst assemblage composition (%)
Age (ka)
2500
2525
2550
2575
2600
2625
2650
2675
2700
2725
2750
2775
2800
Other species
Pbra
Ipal
SpiniSpp.
Iacu
Istr
Inve1
Oeir
Pdal
Ocen
Ilac
Ipat
Htec
Btep + Fmic
Nlab
Ipar
Smir
Ptub

1162 3

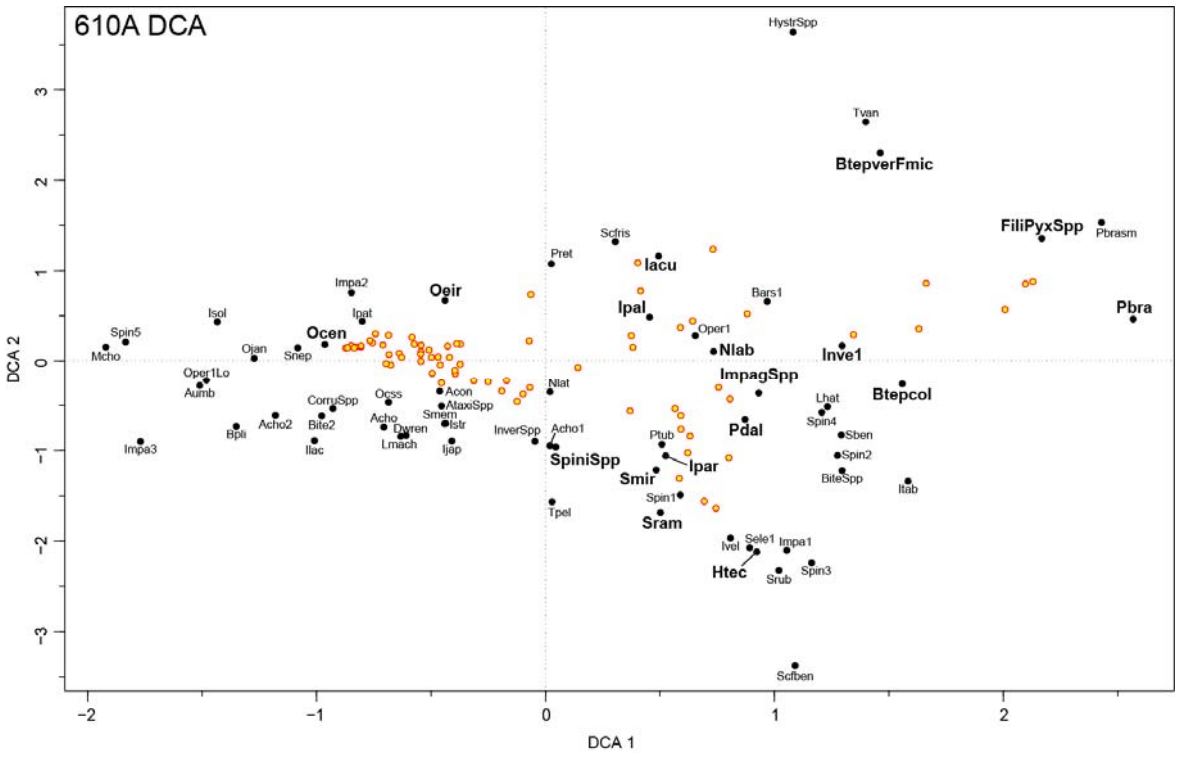

1163

1164 Figure 4

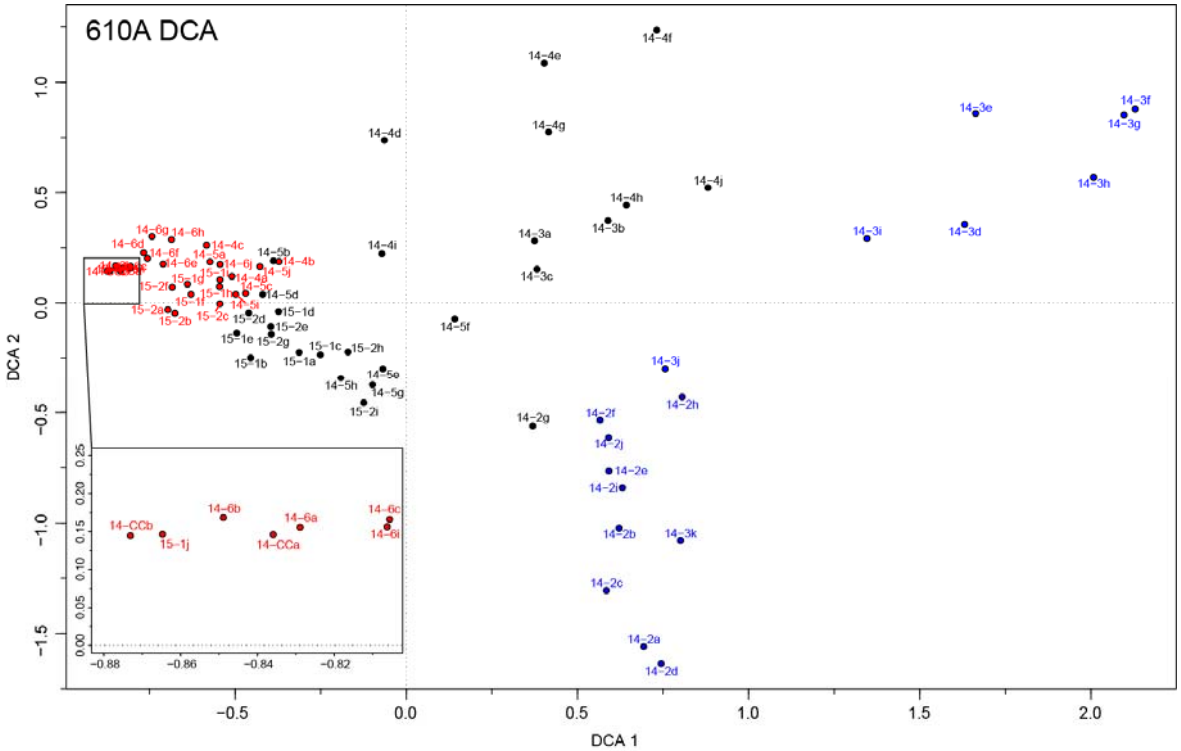

1165

1166 Figure 5

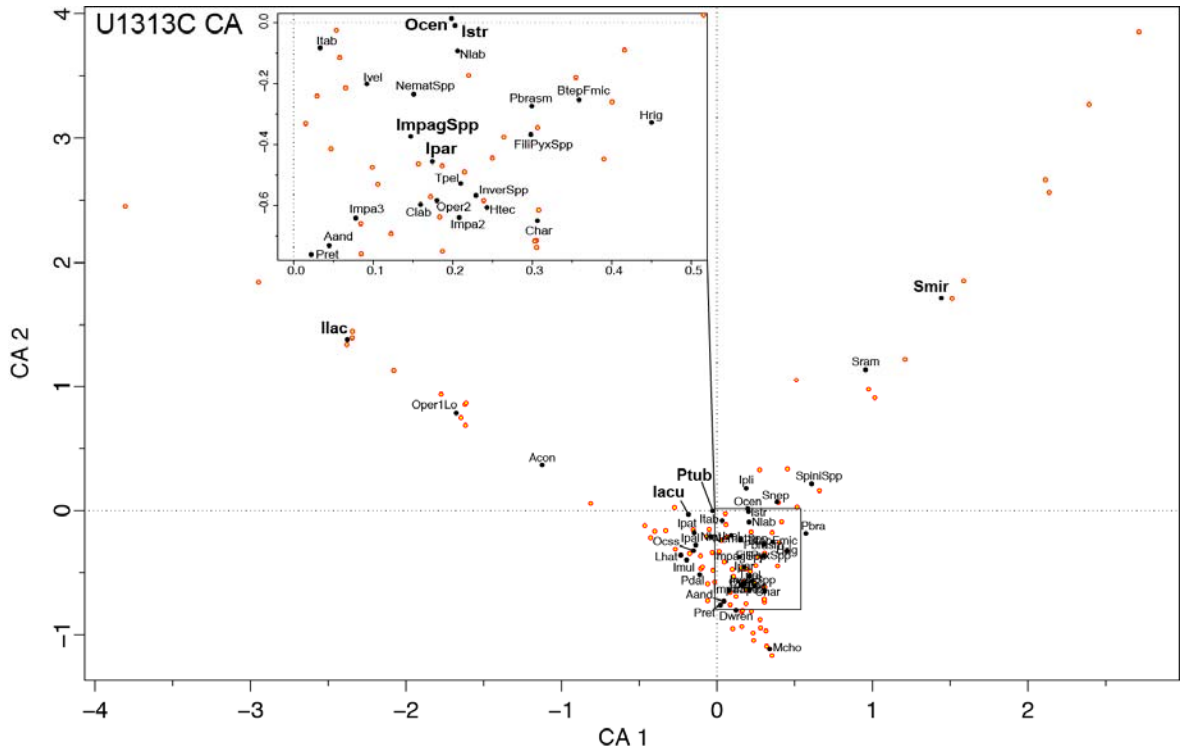

1167

1168 Figure 5

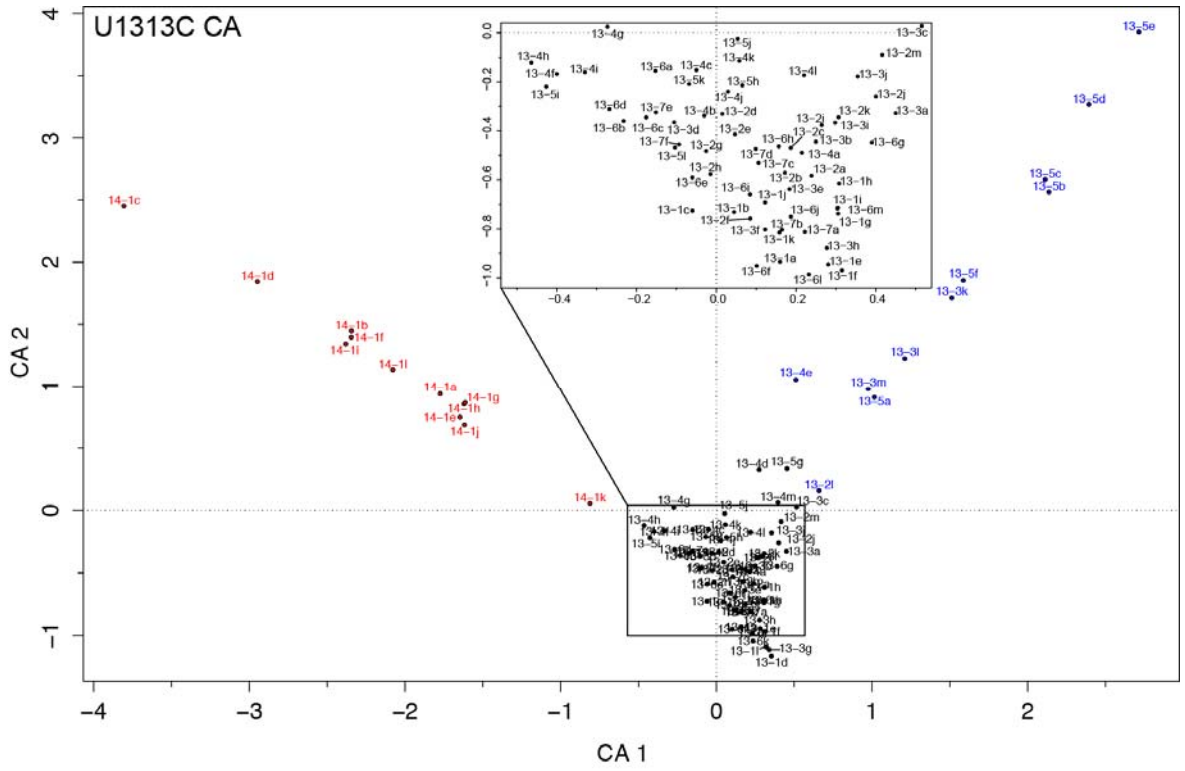
U1313C CA
CA 1
CA 2

Figure 6

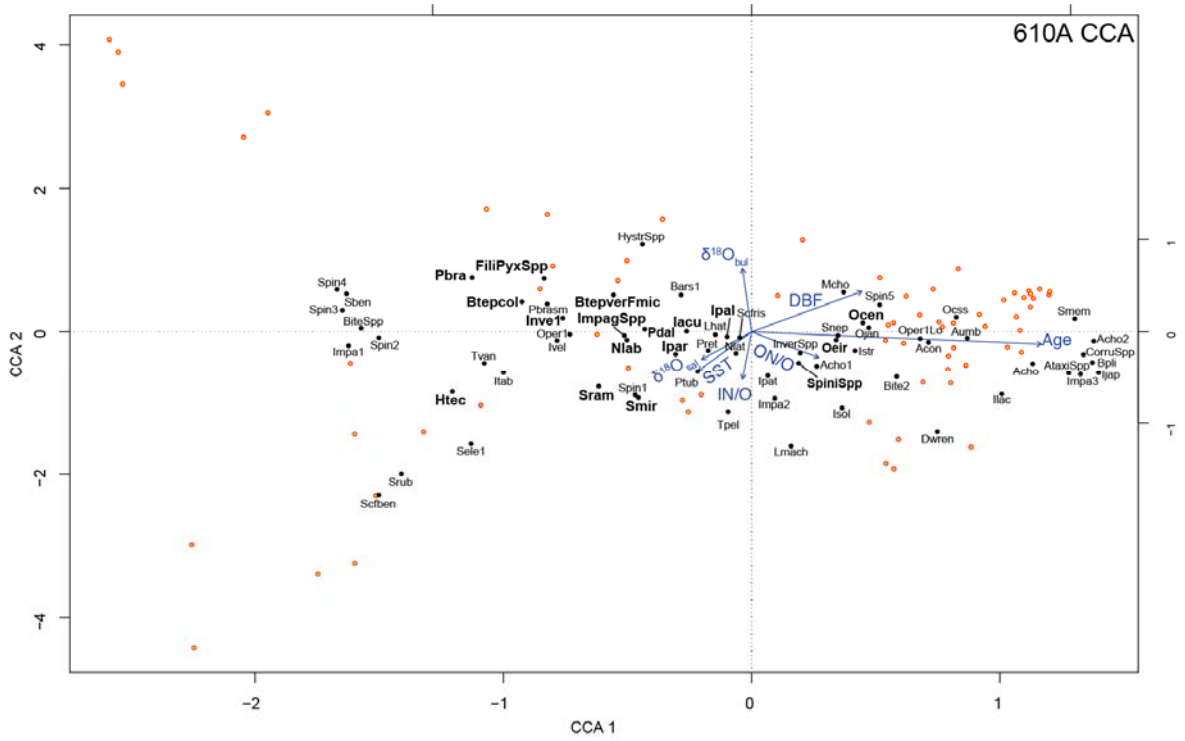
610A CCA
CCA 1
CCA 2
δ18Obul
DBF
Age
δ18Osal
SST
IN/O
ON/O
FiliPyxSpp
Pbra
Btepcol
BtepverFmic
ImpagSpp
Inve1
Nlab
Ipar
Iacu
Ipal
Pdal
Ocen
Oeir
SpiniSpp
Htec
Sram
Smir
HystrSpp
Bars1
Mcho
Spin5
Ocss
Smem
Acho2
CorruSpp
AtaxiSpp
Bpli
Impa3
Acho
Dwren
Lmach
Tpel
Impa2
Isol
Bite2
Sele1
Srub
Scfben

1172 Figure 7

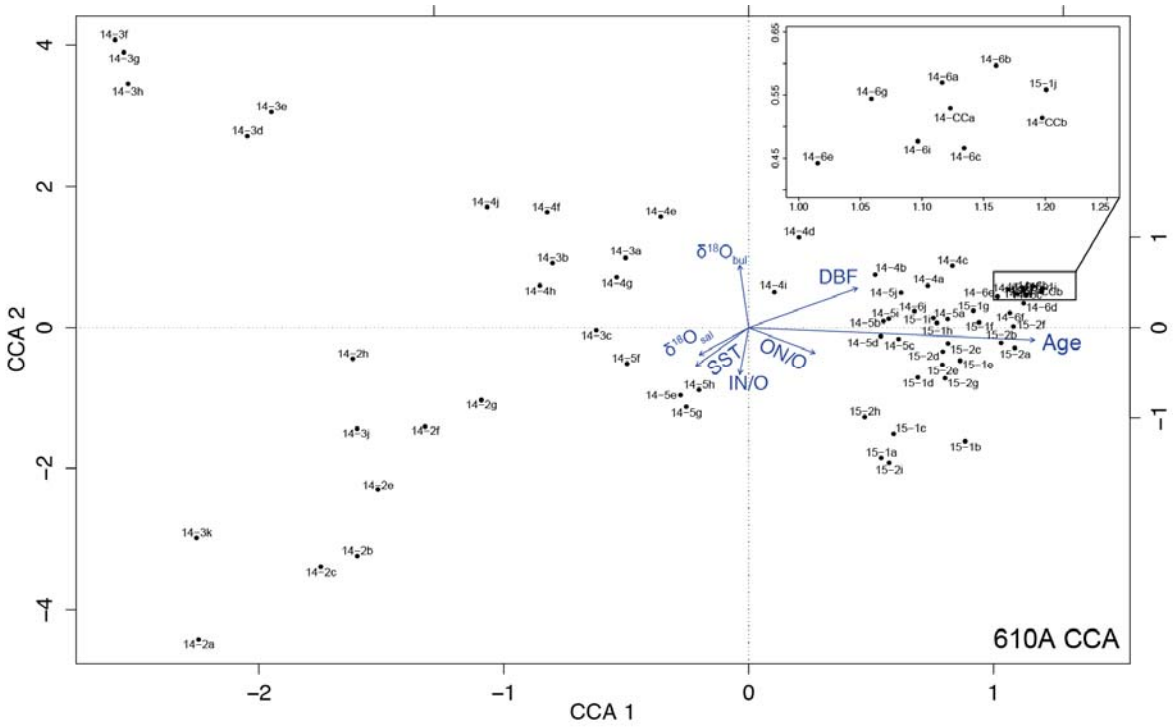

1173

1174 Figure 8

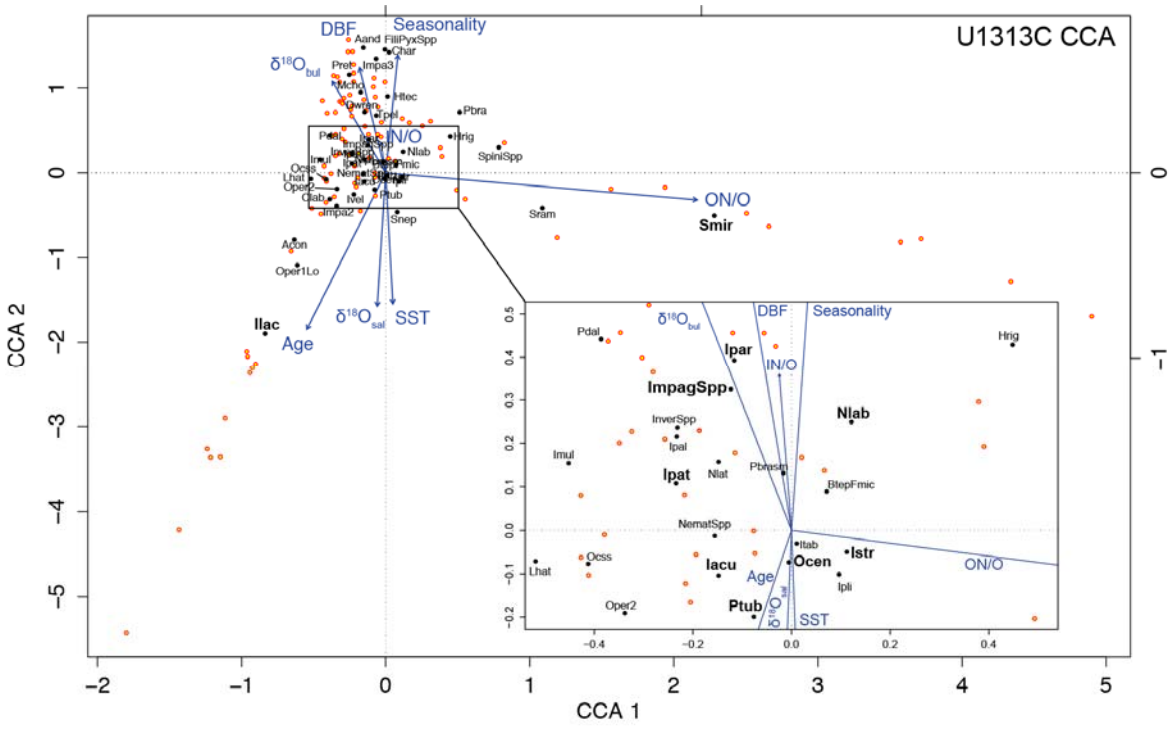

1175

1176 Figure 9

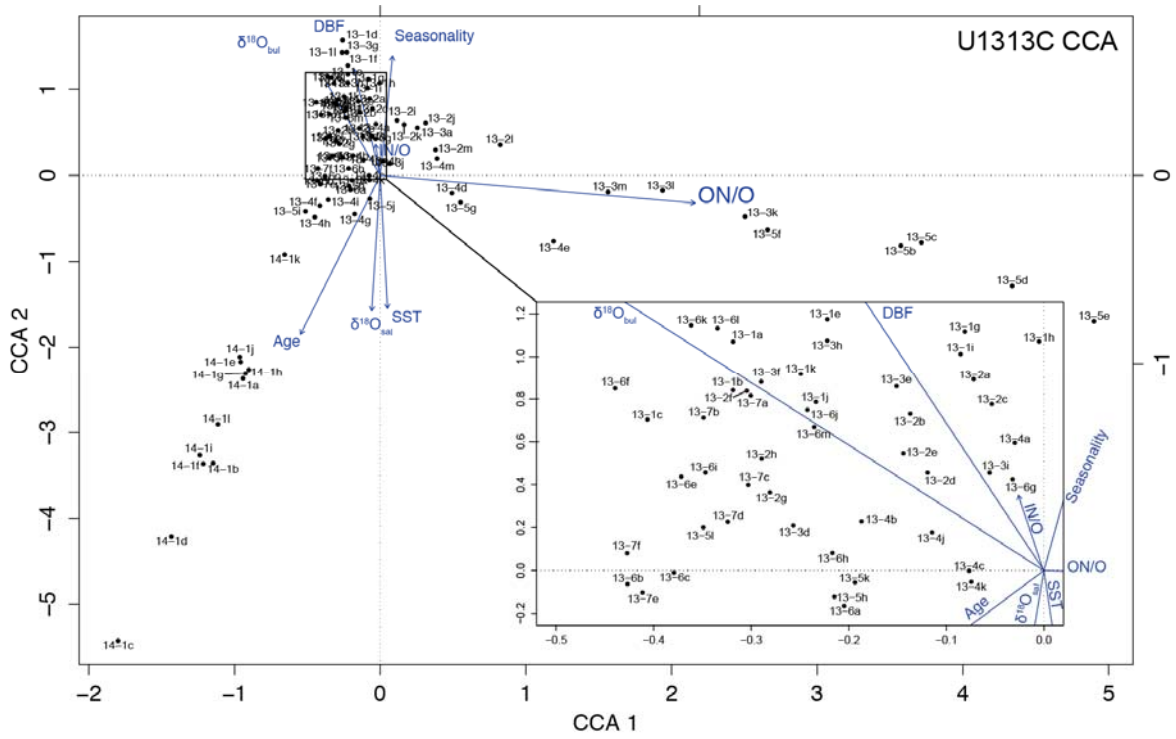

1177

1178 Figure 10

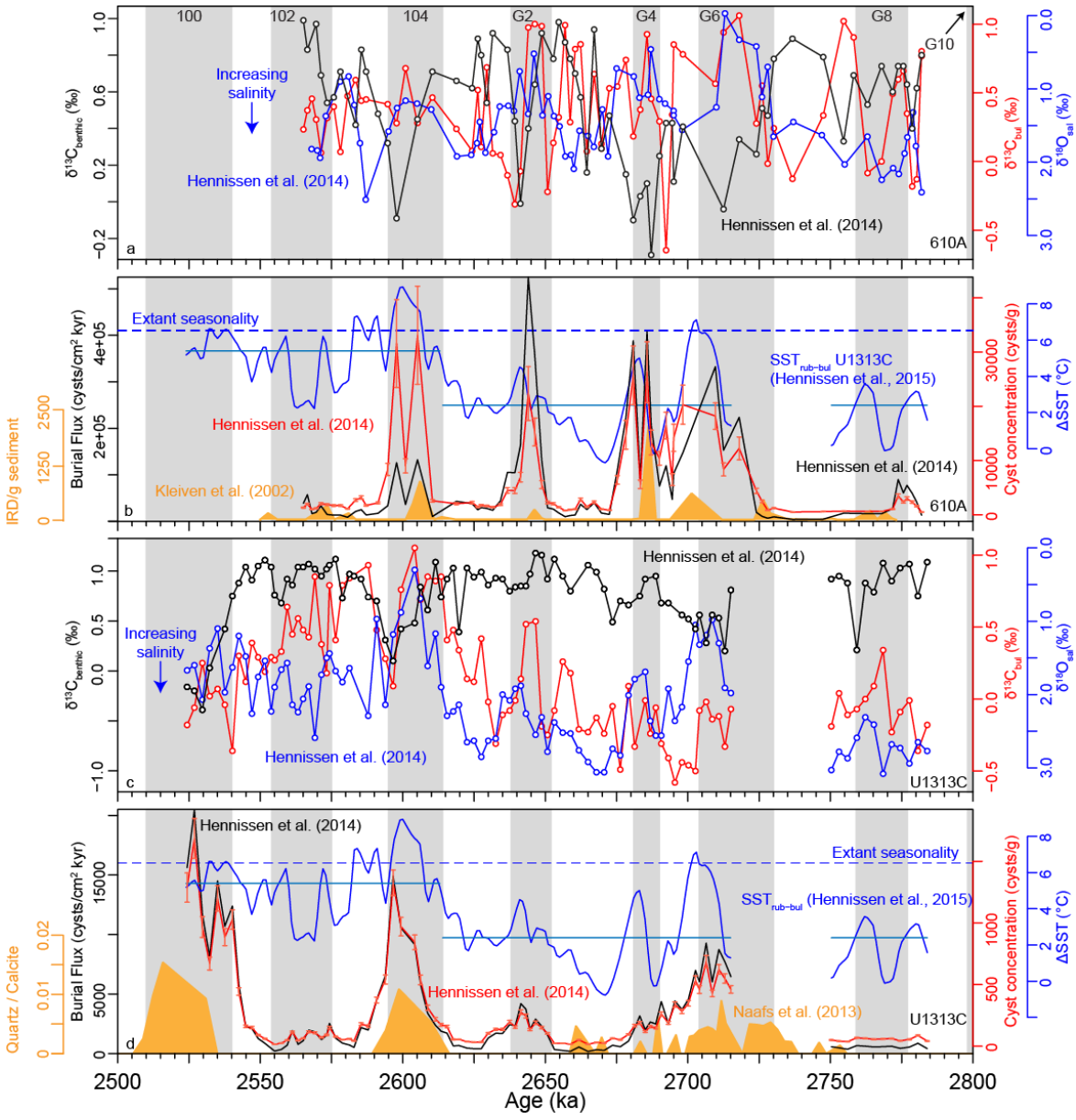

1179

1180 Figure 11

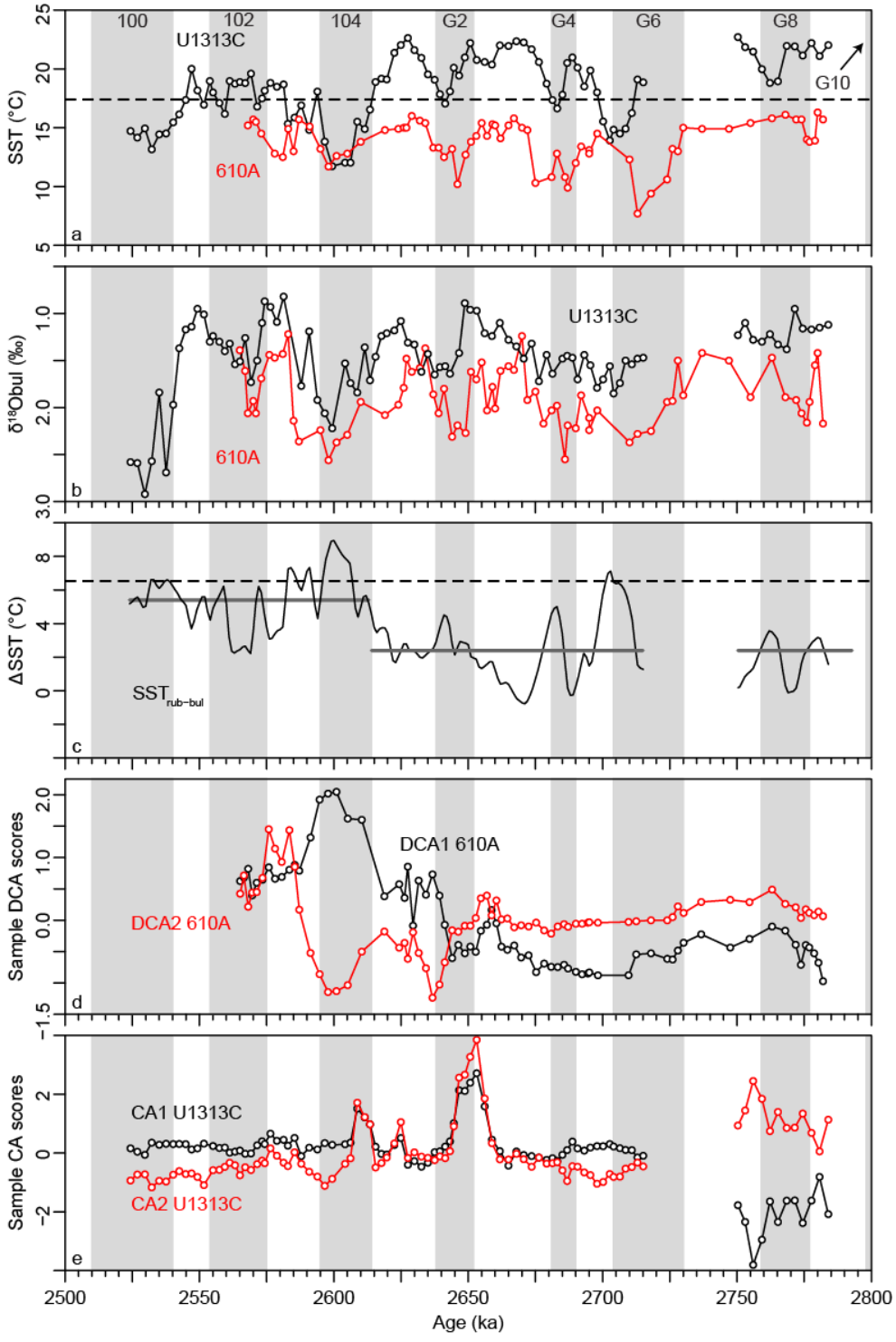

1181

1182 Figure 12

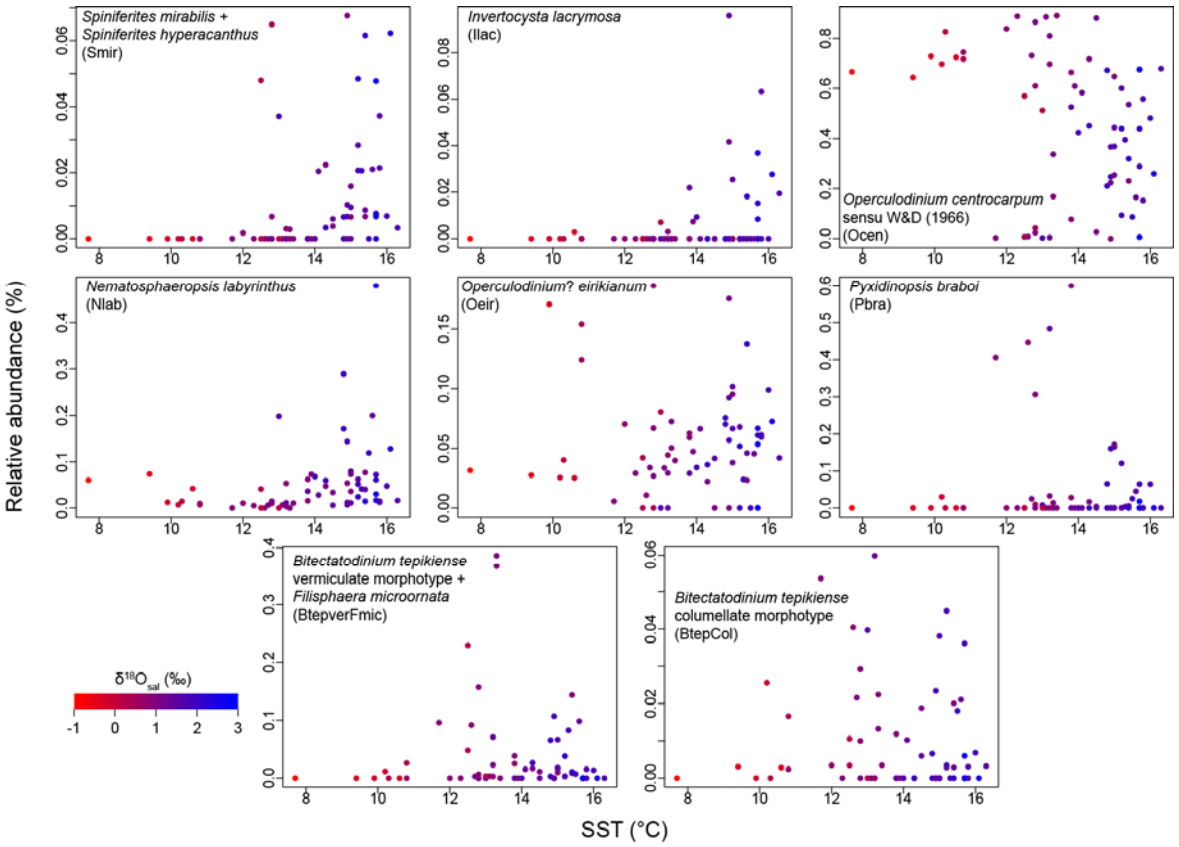

1183

1184 Figure 13

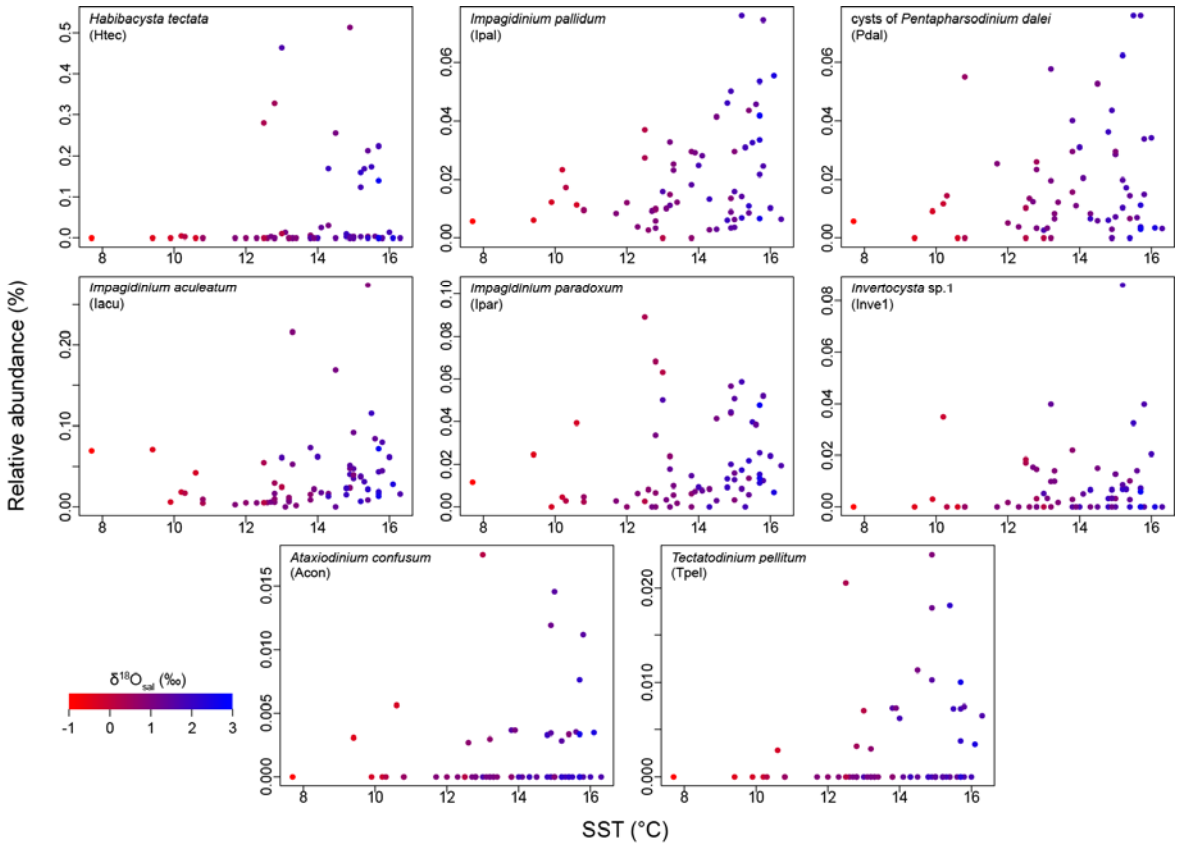

1185

1186 Figure 14

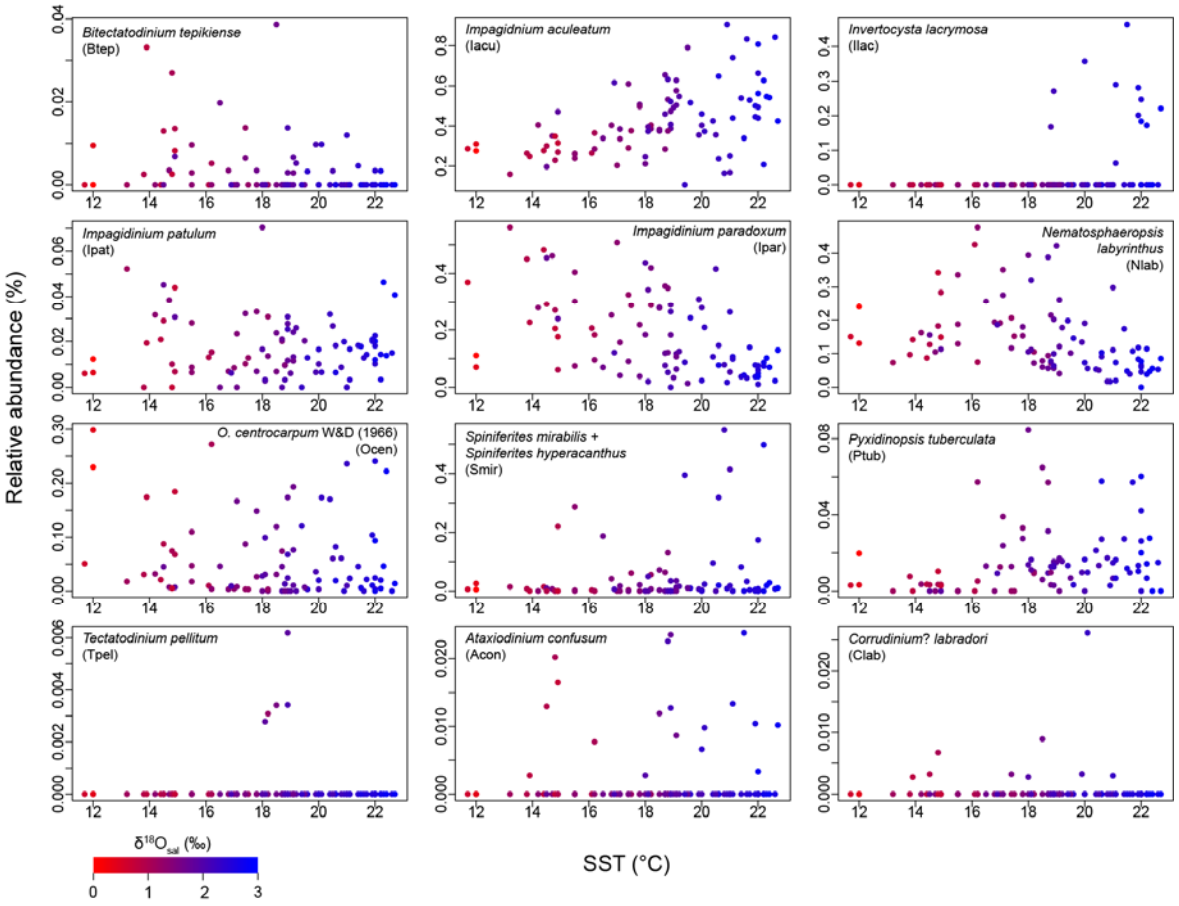
Bitectatodinium tepikiense
(Btep)
Impagidnium aculeatum
(Iacu)
Invertocysta lacrymosa
(Iiac)
Impagidinium patulum
(Ipat)
Impagidinium paradoxum
(Ipar)
Nematosphaeropsis labyrinthus
(Nlab)
O. centrocarpum W&D (1966)
(Ocen)
Spiniferites mirabilis +
Spiniferites hyperacanthus
(Smir)
Pyxidinopsis tuberculata
(Ptub)
Tectatodinium pellitum
(Tpel)
Ataxiodinium confusum
(Acon)
Corrudinium? labradori
(Clab)
Relative abundance (%)
SST (°C)
δ18Osal (‰)

Figure 15

1193 Table 1

Code	Species Name	Code	Species Name
Aand	*Achomosphaera andalousiensis*	Ivel	*Impagidinium velorum*
Acho1	*Achomosphaera* sp. 1	Inve1	*Invertocysta* sp. 1
Acho2	*Achomosphaera* sp. 2	InverSpp	*Invertocysta* spp. indet.
SpiniSpp	*Achomosphaera + Spiniferites* spp. indet.	Itab	*Invertocysta tabulata*
Aumb	*Amiculosphaera umbracula*	Lhat	*Lejeunecysta hatterasensis*
Acho	*Ataxiodinium choane*	Lmach	*Lingulodinium machaerophorum*
Acon	*Ataxiodinium confusum*	Mcho	*Melitasphaeridium choanophorum*
AtaxiSpp	*Ataxiodinium* spp. indet.	NematSpp	*Nematosphaeropsis* spp. indet.
BtepverFmic	*B. tepikiense (vermiculate)+Filisphaera microornata*	Nlab	*Nematosphaeropsis labyrinthus*
Btepcol	*B. tepikiense* (columellate)	Nlat	*Nematosphaeropsis lativittata*
Bpli	*Barssidinium pliocenicum*	Ocen	*Operculodinium centrocarpum* sensu W&D (1966)
Bars1	*Barssidinium* sp. 1	Ocsp	*O. centrocarpum* sensu W&D (1966) short processes
Bite2	*Bitectatodinium* sp. 2	Ocss	*Operculodinium centrocarpum* sensu stricto
BiteSpp	*Bitectatodinium* spp. indet.	Oeir	*Operculodinium eirikianum*
Char	*Corrudinium harlandii*	Ojan	*Operculodinium janduchenei*
Clab	*Corrudinium*? *labradori*	Oper1	*Operculodinium* sp. 1
CorruSpp	*Corrudinium* spp. indet.	Oper1Lo	*Operculodinium*? sp. 1 of Louwye et al. (2004)
Pdal	cysts of *Pentapharsodinium dalei*	Oper2	*Operculodinium* sp. 2
Dwren	*Desotodinium wrennii*	Pbra	*Pyxidinopsis braboi*
DinoSpp	Unidentified dinocysts	Pbrasm	Small *P. braboi / B. tepikiense* (vermiculate)
FilPyxSpp	*Filisphaera/Pyxidinopsis* spp. indet.	Pret	*Pyxidinopsis reticulata*
Hrig	*Hystrichokolpoma rigaudiae*	Ptub	*Pyxidinopsis tuberculata*
Htec	*Habibacysta tectata*	Sben	*Spiniferites bentorii*?
HystrSpp	*Hystrichokolpoma* spp. indet.	Scfben	*Spiniferites* cf. *bentorii*
Iacu	*Impagidinium* aculeatum	Scfris	*Spiniferites* cf. *ristingensis*
Istr	*Impagidinium strialatum*	Sele1	*Selenopemphix* sp. 1
Ijap	*Impagidinium japonicum*	Smem	*Spiniferites membranaceus*
Imul	*Impagidinium multiplexum*	Smir	*Spiniferites mirabilis + Spiniferites hyperacanthus*
Ipal	*Impagidinium pallidum*	Snep	*Selenopemphix nephroides*
Ipar	*Impagidinium paradoxum*	Spin1	*Spiniferites* sp. 1
Ipat	*Impagidinium patulum*	Spin2	*Spiniferites* sp. 2
Ipli	*Impagidinium plicatum*	Spin3	*Spiniferites* sp. 3
Isol	*Impagidinium solidum*	Spin4	*Spiniferites* sp. 4
Impa1	*Impagidinium* sp. 1	Spin5	*Spiniferites* sp. 5
Impa2	*Impagidinium* sp. 2	Sram	*Spiniferites delicatus*? / *ramosus*?
Impa3	*Impagidinium* sp. 3	Srub	*Spiniferites rubinus*
ImpagSpp	*Impagidinium* spp. indet.	Tpel	*Tectatodinium pellitum*
Istr	*Impagidinium strialatum*	Tvan	*Tuberculodinium vancampoae*

1194

Table 2

IN	Dinocysts indicating inner neritic conditions	*Lingulodinium machaerophorum, Operculodinium israelianum, Tectatodinium pellitum, Tuberculodinium vancampoae.*
ON	Dinocysts indicating outer neritic conditions	*Spiniferites bulloides, Spiniferites membranaceus, Spiniferites mirabilis* group, *Spiniferites* spp.
O	Dinocysts indicating oceanic conditions	*Impagidinium aculeatum, Impagidinium paradoxum, Impagidinium* spp. indet., *Impagidinium strialatum, Impagidinium velorum.*

1198

Cyst Code	DCA1	DCA2	DCA3	DCA4	Weight		Cyst Code	DCA1	DCA2	DCA3	DCA4	Weight
(Eigenvalue)	0.499	0.340	0.145	0.134			(Eigenvalue)	0.499	0.340	0.145	0.134	
Acho1	0.019	-0.945	1.231	-1.259	0.317		Itab	1.584	-1.339	0.986	0.850	0.072
Acho2	-1.180	-0.612	1.872	0.897	0.085		Lhat	1.232	-0.514	1.787	-5.586	0.015
SpiniSpp	**0.045**	**-0.961**	**1.216**	**-0.699**	**5.355**		Lmach	-0.633	-0.844	2.722	-4.957	0.153
Aumb	-1.511	-0.282	1.249	0.116	0.233		Mcho	-1.921	0.154	1.515	-3.051	0.003
Acho	-0.706	-0.740	3.442	1.872	0.038		**Nlab**	**0.734**	**0.104**	**0.914**	**1.829**	**3.889**
Acon	-0.462	-0.344	2.113	-1.886	0.108		Nlat	0.020	-0.351	1.403	1.041	0.146
AtaxiSpp	-0.454	-0.507	3.649	4.235	0.007		Ocss	-0.686	-0.466	1.432	0.370	0.212
Btepcol	**1.559**	**-0.262**	**-0.611**	**-0.264**	**0.794**		**Ocen**	**-0.964**	**0.182**	**-0.458**	**0.326**	**30.961**
BtepverFmic	**1.462**	**2.301**	**-0.365**	**-0.601**	**2.415**		**Oeir**	**-0.439**	**0.672**	**0.934**	**-0.716**	**3.657**
Bpli	-1.351	-0.733	1.495	-0.547	0.070		Ojan	-1.272	0.027	-0.401	0.621	0.169
Bars1	0.969	0.660	-0.639	0.568	0.082		Oper1	0.654	0.281	0.382	-0.606	0.075
Bite2	-0.978	-0.618	0.945	-1.403	0.338		Oper1Lo	-1.481	-0.220	-0.394	-1.015	0.057
BiteSpp	1.296	-1.221	-0.274	-4.862	0.014		**Pdal**	**0.872**	**-0.655**	**-0.818**	**-0.132**	**1.246**
CorruSpp	-0.929	-0.535	2.199	1.790	0.021		**Pbra**	**2.567**	**0.464**	**0.020**	**-0.228**	**3.605**
Dwren	-0.609	-0.834	3.075	-4.815	0.003		Pret	0.026	1.074	0.413	0.967	0.035
FiliPyxSpp	**2.168**	**1.356**	**-0.156**	**0.001**	**2.266**		Ptub	0.508	-0.930	1.121	-0.370	0.028
Htec	**0.923**	**-2.118**	**-1.471**	**-0.770**	**4.328**		Snep	-1.082	0.146	1.370	-1.903	0.015
HystrSpp	1.081	3.637	-1.455	-1.478	0.003		Sele1	0.892	-2.071	-0.165	-3.937	0.023
Iacu	**0.494**	**1.160**	**0.761**	**-0.043**	**2.863**		Pbrasm	2.429	1.531	-0.474	-0.970	0.077
Istr	-0.435	-0.702	1.440	0.650	0.105		Sben	1.292	-0.829	-0.148	-1.726	0.071
Ijap	-0.409	-0.895	4.715	2.329	0.007		Scfben	1.090	-3.373	0.438	-2.080	0.010
Ipal	**0.455**	**0.484**	**0.975**	**0.867**	**1.438**		Scfris	0.305	1.319	-0.159	-1.059	0.152
Ipar	**0.525**	**-1.058**	**0.925**	**-1.017**	**1.532**		**Sram**	**0.502**	**-1.686**	**-0.581**	**-1.375**	**1.344**
Ipat	-0.801	0.441	0.942	0.996	0.016		Smem	-0.441	-0.704	1.660	2.238	0.012
Isol	-1.434	0.433	-0.009	0.689	0.010		**Smir**	**0.483**	**-1.214**	**0.788**	**1.130**	**0.911**
Impa1	1.054	-2.102	-1.419	-2.002	0.034		Srub	1.020	-2.324	0.845	-5.798	0.003
Impa2	-0.848	0.757	-1.434	1.127	0.006		Spin1	0.589	-1.489	0.302	-0.324	0.165
Impa3	-1.769	-0.901	1.228	-0.687	0.007		Spin2	1.276	-1.055	-0.204	-3.493	0.047
ImpagSpp	**0.932**	**-0.363**	**1.046**	**1.067**	**0.630**		Spin3	1.163	-2.240	-1.123	-2.737	0.071
Ivel	0.808	-1.966	-1.033	-3.947	0.013		Spin4	1.207	-0.578	0.806	1.328	0.049
Ilac	-1.009	-0.891	3.046	-1.623	0.403		Spin5	-1.834	0.210	1.014	-1.437	0.072
Inve1	**1.296**	**0.168**	**-0.751**	**-0.814**	**0.712**		Tpel	0.029	-1.565	1.412	-2.275	0.194
InverSpp	-0.046	-0.898	1.578	-1.105	0.204		Tvan	1.399	2.645	1.031	1.386	0.007

1199

1200

1201 Table 4

Cyst Code	CA1	CA2	CA3	CA4	Weight		Cyst Code	CA1	CA2	CA3	CA4	Weight
(Eigenvalue)	0.313	0.248	0.126	0.107			(Eigenvalue)	0.313	0.248	0.126	0.107	
Aand	0.045	-0.731	-0.478	0.348	0.004		Itab	0.033	-0.082	0.008	0.231	0.165
Acon	-1.124	0.367	-0.139	-0.971	0.220		Ivel	0.092	-0.201	0.332	-0.282	0.083
BtepFmic	0.359	-0.253	0.101	-0.859	0.310		Lhat	-0.232	-0.360	1.014	0.795	0.007
Char	0.306	-0.650	-0.719	0.435	0.010		Mcho	0.339	-1.114	-2.280	-0.414	0.036
Clab	0.160	-0.597	0.200	-1.648	0.060		NematSpp	0.151	-0.234	0.578	-0.883	0.203
Dwren	0.123	-0.803	-0.745	0.199	0.003		**Nlab**	0.206	-0.092	-0.028	0.106	**13.633**
FiliPyxSpp	0.298	-0.367	1.086	-1.838	0.005		Nlat	-0.040	-0.211	0.015	-0.033	1.115
Hrig	0.450	-0.328	-0.813	-0.296	0.003		**Ocen**	0.198	0.014	0.580	-1.058	**5.507**
Htec	0.243	-0.607	-0.902	0.295	0.077		Ocss	-0.151	-0.324	1.560	-1.043	0.003
Iacu	-0.184	-0.031	0.251	0.204	**39.463**		Oper1Lo	-1.677	0.784	-0.641	-0.937	0.017
Ilac	-2.377	1.383	-0.635	-0.324	**2.920**		Oper2	0.180	-0.584	0.055	-1.087	0.056
Impa2	0.208	-0.638	-0.061	-1.575	0.042		Pbra	0.572	-0.184	-0.915	-0.169	0.092
Impa3	0.078	-0.642	-0.491	0.480	0.014		Pbrasm	0.299	-0.274	0.204	-0.531	0.955
ImpagSpp	0.147	-0.374	-0.259	-0.076	**1.796**		Pdal	-0.111	-0.517	-0.513	-0.575	0.036
Imul	-0.195	-0.398	1.105	0.639	0.033		Pret	0.022	-0.760	-0.504	0.455	0.006
InverSpp	0.229	-0.567	0.255	-1.588	0.037		**Ptub**	-0.028	-0.002	0.131	0.287	**1.479**
Ipal	-0.136	-0.278	-0.191	-0.088	0.710		**Smir**	1.443	1.716	-0.225	0.080	**4.398**
Ipar	0.174	-0.456	-0.559	-0.104	**16.772**		Snep	0.386	0.070	0.807	-1.206	0.014
Ipat	-0.146	-0.179	-0.120	-0.001	**1.570**		SpiniSpp	0.609	0.215	-0.254	0.121	0.605
Ipli	0.188	0.178	0.494	0.209	0.269		Sram	0.956	1.141	-0.153	-0.181	0.263
Istr	0.203	-0.009	0.024	-0.134	**0.990**		Tpel	0.210	-0.528	-0.614	0.452	0.019

1202

1203 Table 5

	Axes	1	2	3	4
610A	DCA	0.499	0.340	0.145	0.134
	DCCA	0.345	0.162	0.069	0.049
U1313C	CA	0.313	0.248	0.126	0.107
	CCA	0.261	0.167	0.068	0.032

1204

1205

Species Code	SST range (°C)		Interpretation of species distribution		References
	610A	U1313C	Plio-Pleistocene (this study)	Modern	
Btepver FMic	10–16	12–22	Cool-tolerant species group, correlated to high seasonality and paleoproductivity. Highest abundances occurred when the Arctic Front was close to 610A. *B. tepikiense* (columellate) possibly more adapted to open-water conditions.	Maximum occurrences in temperate–sub-Arctic conditions of the North Atlantic. Affinity for stratified surface waters with large seasonal SST amplitudes (up to 18°C) and relatively low salinities (30–32). Occurs in seasonally ice-covered areas.	Bakken and Dale (1986); Dale (1985); de Vernal et al. (2005); Head et al. (1989a); Mudie (1992); de Vernal et al. (1998); Rochon et al. (1999); Zonneveld et al. (2013).
BtepCol	9–16	N/A			
Iacu	8–16	12–23	In 610A, maximum of 25% at 15.4°C; >80% in the 20–22°C interval. Negatively correlated to DBF suggesting higher abundance in oligotrophic conditions.	Common in North Atlantic where winter and summer SSTs are >12°C and >18°C respectively and surface salinity exceeds 35 and in central oceanic, oligotrophic domains.	Wall et al. (1977); Rochon et al. (1999); Devillers and de Vernal (2000); De Schepper et al. (2011); Zonneveld et al. (2013).
Ipal	8–16	12–23	The Plio-Pleistocene distribution of *I. pallidum* is not driven by a single factor, although its highest occurrences are associated with a SST of 16 °C, which is warmer than its modern distribution.	Common in the (sub-)Arctic and active oceanic gyre domains. Associated with cold winter conditions and summer SSTs 0–8°C and salinities of 30–34. Indicator of cold open-ocean environments, seasonally ice covered.	de Vernal et al. (1993); Marret and de Vernal (1997); Rochon et al. (1999); Matthiessen and Knies (2001); De Schepper et al. (2011); Zonneveld et al. (2013).
Ipar	8–16	12–23	*Impagidinium paradoxum* oligotrophic species characteristic of higher SSTs (13–14°C), but with a SST optimum lower than that of *I. aculeatum*.	Abundance peaks south of 50°N with winter SSTs >22°C. Distributed in the temperate to equatorial realm, restricted to fully oceanic conditions with low productivity in the upper layers.	Harland (1983); Rochon et al. (1999); Radi and de Vernal (2008); Zonneveld et al. (2013).
Ipat	15–16	12–23	An open-ocean species that occurs over a wide range of hydrographic conditions but abundances do not exceed 7% below 22°C.	Abundance peaks south of 50°N with winter SSTs >22°C. Indicator of temperate–equatorial, open-ocean conditions.	Harland (1983); Rochon et al. (1999); Zonneveld et al. (2013).
Nlab	8–16	12–23	Lower part of binomial distribution of abundance vs SST in 610A, complete binomial abundance vs SST distribution in U1313C suggest highest abundances occur in transitional climatological conditions and dominantly in oligotrophic conditions.	Ubiquitous; sub-polar taxon occurring with winter and summer SSTs of -2°C to ≥15°C and -1°C to ≥20°C and salinities >29. Generally only encountered in full marine settings.	Harland (1983);Turon and Londeix (1988); Baumann and Matthiessen (1992); Rochon et al. (1999); Devillers and de Vernal (2000); Eynaud et al. (2000, 2004); Penaud et al. (2008); Zonneveld et al. (2013).
Ocen	8–16	12–23	High abundances reflect the influence of the NAC. Peak abundance in U1313C during MIS 104 shows a southward shift of the NAC.	Present from middle to high latitudes from the neritic to the oceanic environment with tolerance of wide salinity and SST ranges. Cosmopolitan species that tracks the path of the NAC.	De Schepper et al. (2009, 2013); Dodge and Harland (1991); Harland (1983); Harland (1984); Hennissen et al. (2014, 2015); Rochon et al (1999); Wall et al. (1977); Williams (1971); Zonneveld et al. (2013).
Pdal	8–16	13–20	Cool water species with optimum SSTs ranging from 10.8 to 15.7°C at maximum abundance of 7% in Hole 610A. Present in only very low abundances (<1%) in Hole U1313C.	Occurs when summer SST exceeds 4°C and becomes important under large seasonal SST gradients. High abundances in all but polar realms.	Bakken and Dale (1986); de Vernal et al. (1994, 1997); Harland and Pudsey (1999); Rochon et al. (1999); Zonneveld et al. (2013).
Smir	12–16	12–23	Warm water, oligotrophic distribution with highest abundances (>50 %) in the current study recorded between 21 and 22°C in Hole U1313C. Its isolation in CA and CCA of Hole U1313C suggests incursion of eastern North Atlantic waters.	High abundances in the eastern North Atlantic and off the eastern margins of the US. Warm oceanic species that tolerates waters with a winter SST exceeding 13°C and salinities exceeding 34.5.	Harland (1983); Rochon et al. (1999); Versteegh (1997) ; Zonneveld et al. (2013).
Tpel	11–16	18–19	Inner neritic, thermophilic species.	Coastal subtropical to equatorial species with highest relative abundances in meso- to eutrophic waters.	De Schepper et al. (2011); Versteegh and Zonneveld (1994); Zonneveld et al. (2013).

1206

1207